Small-Signal Stability-Constrained Optimal Power Flow for Inverter Dominant Autonomous Microgrids

Deepak Pullaguram, *Member, IEEE*, Ramtin Madani, *Member, IEEE*, Tuncay Altun, *Member, IEEE*, and Ali Davoudi, *Senior Member, IEEE*

***Abstract*—This article details and solves a small-signal stability-constrained optimal power flow (SSSC-OPF) for inverter-based ac microgrids. To ensure a sufficient stability margin during optimal generation, a small-signal stability constraint is embedded into the conventional OPF formulation. This condition is enforced using a Lyapunov stability equation. A reduced-order model of the microgrid is adopted to alleviate the computational burden involved in solving the resulting SSSC-OPF. Even then, the resulting stability conditions are highly nonlinear and cannot be handled using the existing methods. To tackle the nonconvexity in the SSSC-OPF due to the presence of the nonlinear stability constraint, two distinct convex relaxation approaches, namely semidefinite programming and parabolic relaxations, are developed. A heuristic penalty function is added to the objective function of the relaxed SSSC-OPF, which is solved sequentially to obtain a feasible point. While off-the-shelf tools fail to produce any feasible point within hours, the proposed approach enables us to solve the SSSC-OPF in near real time. The efficacy of the proposed SSSC-OPF is evaluated by performing numerical studies on multiple benchmarks as well as real-time studies on a microgrid system built in a controller/hardware-in-the-loop setup.**

***Index Terms*—AC microgrids, convex optimization, inverters, optimal power flow, relaxation, small-signal stability.**

I. Introduction

MAJORITY of distributed generation units are interfaced with ac microgrids using inverters. A droop mechanism is a well-established decentralized control tool for proportional power sharing among inverters. This control approach alone does not ensure optimal operation or respect operational requirements usually dictated by the optimal power flows (OPFs) paradigms. An OPF-based droop adjustment is given in [1]. Varying droop parameters could cause small-signal stability issues [2], [3]. This article provides an OPF paradigm that respects the small-signal stability margin, generation limits, power flow limits, and voltage constraints.

To enhance the stability margin, supplementary control loops [4], auxiliary stabilizers [5], [6], L_1-adaptive droop control [7], virtual droop frameworks [8], and lead compensators [9] are offered. These control methods are tuned for a selected range of operating points. Alternatively, the voltage, transient, or small-signal stability margin can be enforced by a proper generation dispatch via a holistic stability-constrained optimal power flow formulation. A trajectory-based transient stability-constrained OPF [10] is detailed where, the single machine equivalent method is used to obtain bus equivalent rotor angular trajectory and used as stability constraint. In the same line, to improve the transient stability, a directional derivative-based transient stability constraint is developed and solved using the time-domain staggered direct method. Similarly, voltage stability-constrained OPFs are studied for the conventional power system [11], [12]. In the context of microgrids, a nonlinear optimization-based voltage stability-constrained OPF is developed in [13] and [14] for improving the multimicrogrid voltage stability system. Apart from the transient stability-constrained OPF, a small-signal stability-constrained optimal power flow (SSSC-OPF) problem also has been studied intensively in the context of the conventional power systems [15]–[20].

The SSSC-OPF, with stability constraint dependent on state matrix sensitivities with respect to OPF variables, is detailed in [15] and [16]. The stability constraint is presented as a semidefinite programming (SDP) problem in [17], and the resulting SSSC-OPF is transformed to a nonlinear optimization problem. The SSSC-OPF might lead to infeasible solutions due to its nonconvex nature and the rigid threshold of the stability constraint [17]–[19]. To obtain a feasible solution, sequential quadratic programming and sequential optimization techniques, based on the eigenvalue sensitivity matrix, are presented in [18] and [19], respectively. All these dispatching schemes are developed for the conventional power systems with synchronous generators, and rely on interior-point methods that are sensitive

Manuscript received January 18, 2021; revised May 10, 2021 and June 27, 2021; accepted July 13, 2021. Date of publication August 10, 2021; date of current version February 9, 2022. This work was supported by the Office of Naval Research under Award N00014-18-1-2186 and approved for public release under DCN# 43-8362-21. *(Corresponding author: Ramtin Madani.)*

Deepak Pullaguram is with the University of Texas at Arlington, Arlington, TX 76019 USA. He is now with the National Institute of Technology, Warangal, Telangana 506004, India (e-mail: drp@nitw.ac.in).

Ramtin Madani, Tuncay Altun, and Ali Davoudi are with the University of Texas at Arlington, Arlington, TX 76019 USA (e-mail: ramtin.madani@uta.edu; tuncay.altun@mavs.uta.edu; davoudi@uta.edu).

Color versions of one or more figures in this article are available at https://doi.org/10.1109/TIE.2021.3102454.

Digital Object Identifier 10.1109/TIE.2021.3102454

0278-0046 © 2021 IEEE. Personal use is permitted, but republication/redistribution requires IEEE permission.
See https://www.ieee.org/publications/rights/index.html for more information.

Authorized licensed use limited to: Washington State University. Downloaded on October 11,2022 at 18:27:39 UTC from IEEE Xplore. Restrictions apply.

to initial conditions. Alternatively, bilinear matrix inequalities (BMIs) can be employed to obtain optimal operating points ensuring stability margins. In [20], the SSSC-OPF problem is formulated for the conventional power systems, where the stability constraint is developed using a BMI approach. The formulated SSSC-OPF is convexified using SDP relaxation techniques, which could become computationally inefficient as the number of generators increases. The primary challenge tackled in this article is the accommodation of highly nonlinear matrix inequalities, resulted from enforcing stability conditions in inverter-based microgrids that might not be within the reach of existing solvers. The key contributions can be summarized as follows.

1) An illustrative example shows the susceptibility of OPF solutions for inverter-based ac microgrids to instability.
2) The SSSC-OPF is formulated here by employing a reduced-order dynamical model of inverter-based microgrids [21], and incorporating the Lyapunov stability equations that keeps system spectral abscissa below a certain threshold offering a small-signal stability margin.
3) While the existing optimization tools, e.g., PENBMI [22] and BMILAB [23], could not provide timely solutions for the SSSC-OPF, we solve the resulting nonlinear and nonconvex BMI equations using computationally tractable SDP or parabolic relaxation techniques [24], [25].
4) The SSSC-OPF is solved sequentially through objective penalization, to obtain feasible solutions that are beyond the reach of existing solvers.
5) The penalized, the relaxed SSSC-OPF is experimentally validated for a four-inverter microgrid system in a controller/hardware-in-the-loop (CHIL) environment under various loading scenarios.

A. Notations

The bold-italic upper case ($\boldsymbol{A}$), bold-italic lower case ($\boldsymbol{a}$), and italic lower case (a) indicate matrices, vectors, and scalars, respectively. $\mathbb{R}$ and $\mathbb{C}$ represent sets of real numbers and complex numbers, respectively. $\mathbb{S}^n$ and $\mathbb{H}^n$, respectively, indicate sets of $n \times n$ symmetric matrices and $n \times n$ hermitian matrices. The diagonal matrix with the "$\boldsymbol{a}$" vector of diagonal terms is shown by $[\boldsymbol{a}]$. $[\boldsymbol{a}]^n$ indicates the matrix formed by repeating the vector $\boldsymbol{a}$ for n columns. $(\cdot)^\top$ and $(\cdot)^*$ indicate the transpose and conjugate transpose of a matrix, respectively. $\mathbf{I}^n$ and 0^n indicate identity and zero matrices of size $n \times n$, respectively. The diagonal elements vector of a square matrix is shown by $\mathrm{diag}\{\cdot\}$. The vector or a scalar absolute value is given by $|\cdot|$. The trace of a matrix is shown by $\mathrm{tr}\{\cdot\}$. The frobenius norm of a matrix or a vector is represented by $\|\cdot\|$. The $\mathrm{Re}\{\cdot\}$ and $\mathrm{Im}\{\cdot\}$ indicate real and imaginary parts of the complex numbers, respectively. The notation $\boldsymbol{a} \cdot \boldsymbol{b}$ indicates the element-wise product of vectors $\boldsymbol{a}$ and $\boldsymbol{b}$.

II. Stability-Constrained Optimal Power Flow

A. OPF in AC Microgrids

The ac microgrid has $\mathcal{N} = \{1, 2, \ldots, n\}$ set of buses on the power distribution network, $\mathcal{L} = \{1, 2, \ldots, l\} \subseteq \mathcal{N} \times \mathcal{N}$ set of distribution lines, and $\mathcal{G} = \{1, 2, \ldots, n^{\mathrm{g}}\}$ set of inverters. The vectors of the injected active and reactive powers are $\boldsymbol{p}^{\mathrm{g}} \in \mathbb{R}^{n^{\mathrm{g}} \times 1}$ and $\boldsymbol{q}^{\mathrm{g}} \in \mathbb{R}^{n^{\mathrm{g}} \times 1}$, respectively. $\boldsymbol{d} \in \mathbb{C}^{n^{\mathrm{d}} \times 1}$ is the vector of power demand. An inverter and a load incidence matrix, which locate inverters and loads on the distribution bus, are defined as $\boldsymbol{G} \in \{0,1\}^{n^{\mathrm{g}} \times n}$ and $\hat{\boldsymbol{D}} \in \{0,1\}^{n^{\mathrm{d}} \times n}$. The bus admittance matrix is given by $\boldsymbol{Y} \in \mathbb{C}^{n \times n}$. The $from$ and to admittance matrices are represented as $\vec{\boldsymbol{Y}}$, $\overleftarrow{\boldsymbol{Y}} \in \mathbb{C}^{n \times n}$, and their respective branch-incidence matrices as $\vec{\boldsymbol{L}}$, $\overleftarrow{\boldsymbol{L}} \in \{0,1\}^{l \times n}$. Loads are considered as constant complex impedances, and included as shunt elements in $\boldsymbol{Y}$. $\boldsymbol{v}^{\mathrm{g}} \in \mathbb{C}^{n^{\mathrm{g}} \times 1}$ is the vector of bus voltages at point of coupling, and $\boldsymbol{v}^{\mathrm{b}} \in \mathbb{C}^{n - n^{\mathrm{g}} \times 1}$ is the vector of all remaining buses, such that $\boldsymbol{v} = [\boldsymbol{v}^{\mathrm{g}}, \boldsymbol{v}^{\mathrm{b}}]$ is the vector of all voltages. Finally, $\boldsymbol{v}^{\mathrm{o}}$ is the terminal voltages at inverter output terminals.

The OPF for an ac microgrid is formulated as

$$\text{minimize} \quad \mathrm{h}(\boldsymbol{p}^{\mathrm{g}}) \tag{1a}$$

$$\text{subject to} \quad \boldsymbol{G}^\top(\boldsymbol{p}^{\mathrm{g}} + \mathrm{j}\boldsymbol{q}^{\mathrm{g}}) = \hat{\boldsymbol{D}}^\top \boldsymbol{d} + \mathrm{diag}\{\boldsymbol{v}\boldsymbol{v}^*\boldsymbol{Y}^*\} \tag{1b}$$

$$\mathrm{diag}\{\vec{\boldsymbol{L}}\, \boldsymbol{v}\boldsymbol{v}^*\vec{\boldsymbol{Y}}^*\} \leq \boldsymbol{f}^{\max} \tag{1c}$$

$$\mathrm{diag}\{\overleftarrow{\boldsymbol{L}}\, \boldsymbol{v}\boldsymbol{v}^*\overleftarrow{\boldsymbol{Y}}^*\} \leq \boldsymbol{f}^{\max} \tag{1d}$$

$$\boldsymbol{p}^{\min} \leq \boldsymbol{p}^{g} \leq \boldsymbol{p}^{\max} \tag{1e}$$

$$\boldsymbol{q}^{\min} \leq \boldsymbol{q}^{g} \leq \boldsymbol{q}^{\max} \tag{1f}$$

$$(\boldsymbol{v}^{\min})^2 \leq |\boldsymbol{v}|^2 \leq (\boldsymbol{v}^{\max})^2$$

$$\text{variables} \quad \boldsymbol{v} \in \mathbb{C}^{n \times 1}, \boldsymbol{p}^{\mathrm{g}} \in \mathbb{R}^{n^{\mathrm{g}} \times 1}, \boldsymbol{q}^{\mathrm{g}} \in \mathbb{R}^{n^{\mathrm{g}} \times 1}. \tag{1g}$$

Here, $\mathrm{h}(\boldsymbol{p}^{\mathrm{g}})$ is assumed to be a quadratic cost function

$$\mathrm{h}(\boldsymbol{p}^{\mathrm{g}}) = (\boldsymbol{p}^{\mathrm{g}})^\top [\boldsymbol{c}_2] \tilde{\boldsymbol{p}}^{\mathrm{g}} + \boldsymbol{c}_1^\top \boldsymbol{p}^{\mathrm{g}} + \boldsymbol{c}_0^\top \mathbf{1}^{n_{\mathrm{g}}} \tag{2}$$

where c_2, c_1, and c_0 are the cost coefficients. Quadratic cost functions are widely used in OPF problems even for inverter-based systems [26], [27]. The problem formulation, however, can be solved for any convex formulation of the cost function.

The nodal power balance is enforced using (1b). The line flows are limited in either directions using (1c) and (1d). The active and reactive powers generated by individual inverters are bounded using (1e) and (1f), respectively. The constraint (1g) bounds the voltage magnitude within $[\boldsymbol{v}^{\min}, \boldsymbol{v}^{\max}]$.

B. Case for Stability-Constrained OPF

The OPF alone cannot guarantee a stable operation for a microgrid. Consider the illustrative example of a three-bus, two-inverter microgrid shown in Fig. 2. Primary droop control tunes individual inverters [28], in which the voltage reference ($\boldsymbol{v}^{\mathrm{ref}}$) and frequency reference ($\boldsymbol{\omega}^{\mathrm{ref}}$) are obtained using

$$\boldsymbol{\omega}^{\mathrm{ref}} = \omega_{\mathrm{nom}} - \boldsymbol{m}^p \cdot \boldsymbol{p} + \boldsymbol{m}^p \cdot \boldsymbol{p}^{\mathrm{opt}} \tag{3}$$

$$\boldsymbol{v}^{\mathrm{ref}} = \boldsymbol{v}^{\mathrm{opt}} + \boldsymbol{n}^q \cdot \boldsymbol{q}^{\mathrm{opt}} - \boldsymbol{n}^q \cdot \boldsymbol{q}. \tag{4}$$

$\boldsymbol{p}$ and $\boldsymbol{q}$ are the vectors of filtered active and reactive power of the inverter, respectively. $\boldsymbol{p}^{\mathrm{opt}}$, $\boldsymbol{q}^{\mathrm{opt}}$, and $\boldsymbol{v}^{\mathrm{opt}}$ are the vectors of active power, reactive power, and voltages set points provided by the OPF. $\boldsymbol{m}^p$ and $\boldsymbol{n}^q$ are the vectors of $p - \omega$ and $q - v$

Authorized licensed use limited to: Washington State University. Downloaded on October 11,2022 at 18:27:39 UTC from IEEE Xplore. Restrictions apply.

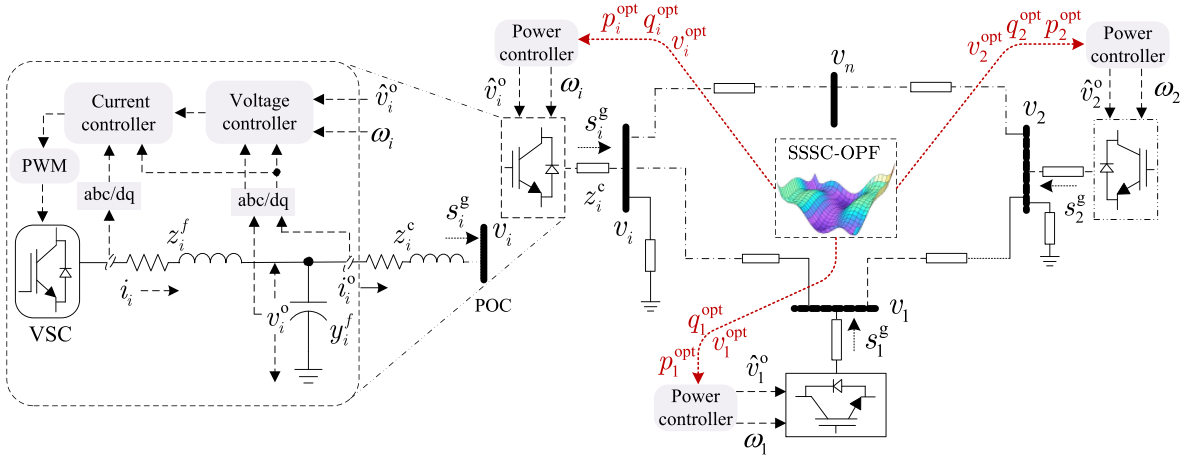

Fig. 1. AC microgrid schematic, inverter control, SSSC-OPF optimization, and data flow.

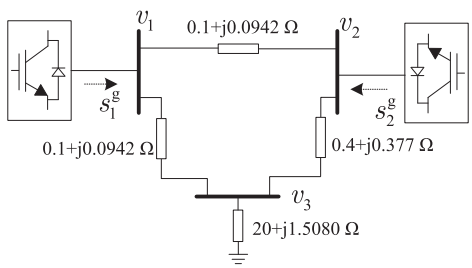

Fig. 2. three-bus, two-inverter ac microgrid example system with line and load parameters.

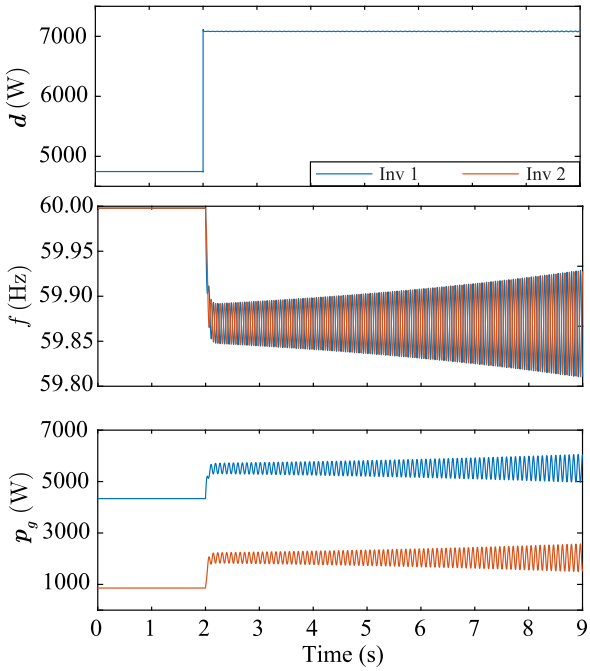

Fig. 3. Unstable microgrid operation with the conventional OPF but without enforcing any stability constraint.

droop relations, respectively. Droop constants, used in the local primary control of inverters, are chosen as $m^p = 6.5 \times 10^{-4}$ (for the active power-frequency droop) and $n^q = 1.3 \times 10^{-3}$ (for the reactive power-voltage droop). Respective cost functions of inverters are formulated as $\mathrm{h}(p_1^{\mathrm{g}}) = 0.1(p_1^{\mathrm{g}})^2 + 20p_1^{\mathrm{g}}$ and $\mathrm{h}(p_2^{\mathrm{g}}) = 0.35(p_2^{\mathrm{g}})^2 + 20p_2^{\mathrm{g}}$. The microgrid operation, under the conventional OPF, is shown in Fig. 3. When the power demand at bus 3 changes at $t = 2$ s, the microgrid becomes unstable. This example illustrates the need to incorporate stability constraints in the OPF formulation. Next, additional constraints concerning the system stability, inspired by the microgrid dynamics in [2], are needed to strengthen (1).

C. Incorporating Stability Constraint

To formulate the stability constraint, first, the microgrid is modeled as a set of differential-algebraic equations

$$\dot{\boldsymbol{x}} = \boldsymbol{f}(\boldsymbol{x}, \boldsymbol{z}) \tag{5a}$$

$$0 = \boldsymbol{g}(\boldsymbol{x}, \boldsymbol{z}) \tag{5b}$$

where $\boldsymbol{f}$ and $\boldsymbol{g}$ represent the vectors of nonlinear differential and algebraic equations of a microgrid, respectively. $\boldsymbol{x}$ and $\boldsymbol{z}$ are the vectors of state and algebraic variables of size n_{x} and n_{z}, respectively. To reduce the computational burden, a third-order inverter model [21] is adopted. The voltage and current controllers with an *LC* filter in Fig. 1 have a high closed-loop bandwidth compared to the power controller module, and one can assume that these control loops reach a quasi-steady-state fast. Thus, the vector of differential equations, $\boldsymbol{f}$, with state variables $\boldsymbol{x} = [\boldsymbol{p}^\top, \boldsymbol{q}^\top, \boldsymbol{\delta}^\top]^\top \in \mathbb{R}^{n_{\mathrm{x}} \times 1}$, is composed of

$$\dot{\boldsymbol{p}} = -\boldsymbol{\omega}^c \cdot \boldsymbol{p} + \boldsymbol{\omega}^c \cdot \mathrm{Re}\{\boldsymbol{v}^{\mathrm{o}} \cdot (\boldsymbol{i}^{\mathrm{o}})^*\} \tag{6a}$$

$$\dot{\boldsymbol{q}} = -\boldsymbol{\omega}^c \cdot \boldsymbol{q} + \boldsymbol{\omega}^c \cdot \mathrm{Im}\{\boldsymbol{v}^{\mathrm{o}} \cdot (\boldsymbol{i}^{\mathrm{o}})^*\} \tag{6b}$$

$$\dot{\boldsymbol{\delta}} = (\boldsymbol{\omega} - \omega_{\mathrm{com}})\omega_{\mathrm{nom}}. \tag{6c}$$

Here, $\boldsymbol{\omega}^c \in \mathbb{R}^{n^{\mathrm{g}} \times 1}$ is the cutoff frequency of low-pass filters used in power controller modules (see Fig. 1). $\boldsymbol{p} \in \mathbb{R}^{n^{\mathrm{g}} \times 1}$ and $\boldsymbol{q} \in \mathbb{R}^{n^{\mathrm{g}} \times 1}$ are the vectors of filtered active and reactive powers, respectively. ω_{nom} and $\boldsymbol{\omega}$ are the microgrid nominal frequency and inverter operating frequency, respectively. $\boldsymbol{v}^{\mathrm{o}} \in \mathbb{C}^{n^{\mathrm{g}} \times 1} =$

Authorized licensed use limited to: Washington State University. Downloaded on October 11,2022 at 18:27:39 UTC from IEEE Xplore. Restrictions apply.

$\boldsymbol{v}^{\mathrm{od}} + \mathrm{j}\boldsymbol{v}^{\mathrm{oq}}$ and $\boldsymbol{i}^{\mathrm{o}} \in \mathbb{C}^{n^{\mathrm{g}}\times 1} = \boldsymbol{i}^{\mathrm{od}} + \mathrm{j}\boldsymbol{i}^{\mathrm{oq}}$ are the inverter terminal's voltage and current, respectively. $\boldsymbol{\delta}$ is the vector of inverter power angles with respect to a common reference, usually the inverter at bus 1 (i.e., $\omega_{\mathrm{com}} = \omega_1$). The operating frequency $\boldsymbol{\omega}$ is obtained using

$$\boldsymbol{\omega} = \omega_{\mathrm{nom}} - \boldsymbol{m}^p \cdot \boldsymbol{p} + \boldsymbol{m}^p \cdot \boldsymbol{p}^{\mathrm{opt}} \tag{7}$$

where $\boldsymbol{p}^{\mathrm{opt}}$ is the active power set-point provided by the OPF, and $\boldsymbol{m}^p$ is the $p-\omega$ droop constant.

The vector of algebraic equations $\boldsymbol{g}$, with algebraic variables $\boldsymbol{z} = [(\boldsymbol{i}^{\mathrm{od}})^\top, (\boldsymbol{i}^{\mathrm{oq}})^\top]^\top \in \mathbb{R}^n_{\mathrm{z}} \times 1$, are given by

$$\boldsymbol{i}^{\mathrm{od}} = \mathrm{Re}\{\check{\boldsymbol{Y}}(\boldsymbol{v}^{\mathrm{o}} - \boldsymbol{i}^{\mathrm{o}} \cdot \boldsymbol{z}^c)\} \tag{8a}$$

$$\boldsymbol{i}^{\mathrm{oq}} = \mathrm{Im}\{\check{\boldsymbol{Y}}(\boldsymbol{v}^{\mathrm{o}} - \boldsymbol{i}^{\mathrm{o}} \cdot \boldsymbol{z}^c)\}. \tag{8b}$$

$\check{\boldsymbol{Y}}$ is the Kron-reduced admittance matrix of the distribution network [21], $\boldsymbol{z}^{\mathrm{c}}$ is the impedance of the line connecting an inverter to the power distribution network, and

$$\boldsymbol{v}^{\mathrm{o}} = (\boldsymbol{v}^{\mathrm{opt}} + \boldsymbol{n}^q \cdot \boldsymbol{q}^{\mathrm{opt}} - \boldsymbol{n}^q \cdot \boldsymbol{q}) \cdot (\cos\boldsymbol{\delta} + \mathrm{j}\sin\boldsymbol{\delta}) \tag{9}$$

where $\boldsymbol{q}^{\mathrm{opt}}$ and $\boldsymbol{v}^{\mathrm{opt}}$ are the optimal reactive power and voltage set-points provided by the OPF, respectively. $\boldsymbol{n}^q$ is $q-v$ droop constant. (10)–(13) shown at bottom of this page.

Proposition 1: Consider a microgrid system defined by (5a) and (5b). Define $\hat{\boldsymbol{A}} \in \mathbb{R}^{n_{\mathrm{x}}\times n_{\mathrm{x}}}$ as the state matrix

$$\hat{\boldsymbol{A}} = \boldsymbol{A}(\boldsymbol{i}^{\mathrm{od}}, \boldsymbol{i}^{\mathrm{oq}}, \boldsymbol{\delta}, \boldsymbol{q}) - \boldsymbol{B}(\boldsymbol{\delta}, \boldsymbol{q})(\boldsymbol{D})^{-1}\boldsymbol{C}(\boldsymbol{\delta}, \boldsymbol{q}). \tag{14}$$

where $\boldsymbol{A}(\boldsymbol{i}^{\mathrm{od}}, \boldsymbol{i}^{\mathrm{oq}}, \boldsymbol{\delta}, \boldsymbol{q}) = \frac{\partial \boldsymbol{f}}{\partial \boldsymbol{x}}$, $\boldsymbol{B}(\boldsymbol{\delta}, \boldsymbol{q}) = \frac{\partial \boldsymbol{f}}{\partial \boldsymbol{z}}$, $\boldsymbol{C}(\boldsymbol{\delta}, \boldsymbol{q}) = \frac{\partial \boldsymbol{g}}{\partial \boldsymbol{x}}$, and $\boldsymbol{D} = \frac{\partial \boldsymbol{g}}{\partial \boldsymbol{z}}$ are given by (10)–(13), and the matrix $\boldsymbol{M}^{\mathrm{p}}$ in (10) is defined as

$$\boldsymbol{M}^{\mathrm{p}} = \begin{bmatrix} -m_1^{\mathrm{p}} & m_2^{\mathrm{p}} & 0 & \cdots & 0 \\ -m_1^{\mathrm{p}} & 0 & m_3^{\mathrm{p}} & \cdots & 0 \\ \vdots & \vdots & \vdots & \ddots & 0 \\ -m_1^{\mathrm{p}} & 0 & 0 & \cdots & m_{n^g}^{\mathrm{p}} \end{bmatrix} \tag{15}$$

where each m_i^{p} indicates the droop constant of the ith inverter, and $\check{\boldsymbol{G}}$ and $\check{\boldsymbol{B}}$ are, respectively, the real and imaginary components of the Kron-reduced admittance matrix $\check{\boldsymbol{Y}}$. The small-signal stability of the microgrid, with a minimum decay rate($\propto$ damping ratio) of η, can be assured [29] iff there exists a symmetric positive definite matrix $\boldsymbol{M}$ that satisfies

$$\hat{\boldsymbol{A}}^\top \boldsymbol{M} + \boldsymbol{M}\hat{\boldsymbol{A}} \preceq -2\eta \boldsymbol{M}. \tag{16}$$

Proof: Linearizing (5a) and (5b) at the operating point $(\boldsymbol{x}_0, \boldsymbol{z}_0)$, using the Taylor series expansion, gives

$$\begin{bmatrix} \Delta\dot{\boldsymbol{x}} \\ \\ 0 \end{bmatrix} = \begin{bmatrix} \frac{\partial \boldsymbol{f}}{\partial \boldsymbol{x}} & \frac{\partial \boldsymbol{f}}{\partial \boldsymbol{z}} \\ \\ \frac{\partial \boldsymbol{g}}{\partial \boldsymbol{x}} & \frac{\partial \boldsymbol{g}}{\partial \boldsymbol{z}} \end{bmatrix} \begin{bmatrix} \Delta\boldsymbol{x} \\ \\ \Delta\boldsymbol{z} \end{bmatrix}. \tag{17}$$

The partial differential matrices $\frac{\partial \boldsymbol{f}}{\partial \boldsymbol{x}}$, $\frac{\partial \boldsymbol{f}}{\partial \boldsymbol{z}}$, $\frac{\partial \boldsymbol{g}}{\partial \boldsymbol{x}}$, and $\frac{\partial \boldsymbol{g}}{\partial \boldsymbol{z}}$ in (17) are given by (10)–(13), respectively. Eliminating the algebraic variables $\boldsymbol{z}$, (17) can be reformulated [30] as

$$\dot{\boldsymbol{x}} = \hat{\boldsymbol{A}}\boldsymbol{x}. \tag{18}$$

Consider a Lyapunov energy function, $V = \boldsymbol{x}^\top \boldsymbol{M}\boldsymbol{x}$, where $\boldsymbol{M} \in \mathbb{S}^{n_{\mathrm{x}}}$ is a symmetric positive definite matrix. Differentiating V, one has

$$\begin{aligned} \dot{V} &= \dot{\boldsymbol{x}}^\top \boldsymbol{M}\boldsymbol{x} + \boldsymbol{x}^\top \boldsymbol{M}\dot{\boldsymbol{x}} = (\hat{\boldsymbol{A}}\boldsymbol{x})^\top \boldsymbol{M}\boldsymbol{x} + \boldsymbol{x}^\top \boldsymbol{M}\hat{\boldsymbol{A}}\boldsymbol{x} \\ &= \boldsymbol{x}^\top (\hat{\boldsymbol{A}}^\top \boldsymbol{M} + \boldsymbol{M}\hat{\boldsymbol{A}})\boldsymbol{x}. \end{aligned} \tag{19}$$

For the microgrid to have a minimum damping (or decay rate) η, the necessary condition on the Lyapunov function [29] is

$$\dot{V} < -2\eta E. \tag{20}$$

From (19) and (20), one can conclude (16), and the proof of Proposition 1 is completed. ■

From Proposition 1, the microgrid stability can be maintained by choosing η to be a small positive constant. η should be properly chosen, as a large η could lead to an infeasible solution, and a small η might not provide sufficient damping. Herein, η is selected in the range of $[0.5,\ 5]$.

To interlink the inverter internal variables with the OPF variables, additional constraints are formulated as

$$\boldsymbol{v}^{\mathrm{g}} = (\boldsymbol{v}^{\mathrm{ref}} - \boldsymbol{n}^q \cdot \boldsymbol{q}) \cdot (\cos\boldsymbol{\delta} + \mathrm{j}\sin\boldsymbol{\delta}) - \boldsymbol{i}^{\mathrm{o}} \cdot \boldsymbol{z}^c \tag{21}$$

$$\boldsymbol{i}^{\mathrm{o}} = \check{\boldsymbol{Y}}\boldsymbol{v}^{\mathrm{g}} \tag{22}$$

$$\boldsymbol{p} + \mathrm{i}\boldsymbol{q} = \mathrm{diag}\{\boldsymbol{i}^{\mathrm{o}}(\boldsymbol{i}^{\mathrm{o}})^*[\boldsymbol{z}^{\mathrm{c}}]\} + \boldsymbol{p}^g + \mathrm{i}\boldsymbol{q}^g. \tag{23}$$

$$\frac{\partial \mathbf{f}}{\partial \boldsymbol{x}} = \begin{bmatrix} -[\boldsymbol{\omega}^{\mathrm{c}}] & -\left[\boldsymbol{\omega}^{\mathrm{c}} \cdot \boldsymbol{n}^q \cdot (\boldsymbol{i}^{\mathrm{oq}} \cdot \sin\boldsymbol{\delta} + \boldsymbol{i}^{\mathrm{od}} \cdot \cos\boldsymbol{\delta})\right] & -\left[\boldsymbol{\omega}^{\mathrm{c}} \cdot (\boldsymbol{v}^{\mathrm{ref}} - \boldsymbol{n}^q \cdot \boldsymbol{q}) \cdot (\boldsymbol{i}^{\mathrm{od}} \cdot \sin\boldsymbol{\delta} - \boldsymbol{i}^{\mathrm{oq}} \cdot \cos\boldsymbol{\delta})\right] \\ 0^{n^{\mathrm{g}}} & \left[\boldsymbol{\omega}^{\mathrm{c}} \cdot \boldsymbol{n}^{\mathrm{q}} \cdot (\boldsymbol{i}^{\mathrm{oq}} \cdot \cos\boldsymbol{\delta} - \boldsymbol{i}^{\mathrm{od}} \cdot \sin\boldsymbol{\delta}) - \boldsymbol{\omega}^{\mathrm{c}}\right] & \left[\boldsymbol{\omega}^{\mathrm{c}} \cdot (\boldsymbol{v}^{\mathrm{ref}} - \boldsymbol{n}^{\mathrm{q}} \cdot \boldsymbol{q}) \cdot (\boldsymbol{i}^{\mathrm{od}} \cdot \cos\boldsymbol{\delta} + \boldsymbol{i}^{\mathrm{oq}} \cdot \sin\boldsymbol{\delta})\right] \\ \boldsymbol{M}^{\mathrm{p}} & 0^{n^{\mathrm{g}}-1} & 0^{n^{\mathrm{g}}-1} \end{bmatrix} \tag{10}$$

$$\frac{\partial \mathbf{f}}{\partial \boldsymbol{z}} = \begin{bmatrix} \left[\boldsymbol{\omega}^{\mathrm{c}} \cdot (\boldsymbol{v}^{\mathrm{ref}} - \boldsymbol{n}^{\mathrm{q}} \cdot \boldsymbol{q}) \cdot \cos\boldsymbol{\delta}\right] & \left[\boldsymbol{\omega}^{\mathrm{c}} \cdot (\boldsymbol{v}^{\mathrm{ref}} - \boldsymbol{n}^{\mathrm{q}} \cdot \boldsymbol{q}) \cdot \sin\boldsymbol{\delta}\right] \\ \left[\boldsymbol{\omega}^{\mathrm{c}} \cdot (\boldsymbol{v}^{\mathrm{ref}} - \boldsymbol{n}^{\mathrm{q}} \cdot \boldsymbol{q}) \cdot \sin\boldsymbol{\delta}\right] & -\left[\boldsymbol{\omega}^{\mathrm{c}} \cdot (\boldsymbol{v}^{\mathrm{ref}} - \boldsymbol{n}^{\mathrm{q}} \cdot \boldsymbol{q}) \cdot \cos\boldsymbol{\delta}\right] \\ 0^{n\mathrm{g}-1} & 0^{n\mathrm{g}-1} \end{bmatrix} \tag{11}$$

$$\frac{\partial \mathbf{g}}{\partial \boldsymbol{x}} = \begin{bmatrix} 0^{n_{\mathrm{g}}} & (\check{\boldsymbol{G}} \cdot [\boldsymbol{n}^{\mathrm{q}} \cdot \cos\boldsymbol{\delta}]^{n^{\mathrm{g}}} - \check{\boldsymbol{B}} \cdot [\boldsymbol{n}^{\mathrm{q}} \cdot \sin\boldsymbol{\delta}]^{n^{\mathrm{g}}}) & \check{\boldsymbol{G}} \cdot [(\boldsymbol{v}^{\mathrm{ref}} - \boldsymbol{n}^{\mathrm{q}} \cdot \boldsymbol{q}) \cdot \sin\boldsymbol{\delta}]^{n^{\mathrm{g}}} + \check{\boldsymbol{B}}[(\boldsymbol{v}^{\mathrm{ref}} - \boldsymbol{n}^{\mathrm{q}} \cdot \boldsymbol{q}) \cdot \cos\boldsymbol{\delta}]^{n^{\mathrm{g}}} \\ 0^{n_{\mathrm{g}}} & (\check{\boldsymbol{G}} \cdot [\boldsymbol{n}^{\mathrm{q}} \cdot \sin\boldsymbol{\delta}]^{n^{\mathrm{g}}} + \check{\boldsymbol{B}} \cdot [\boldsymbol{n}^{\mathrm{q}} \cdot \cos\boldsymbol{\delta}]^{n^{\mathrm{g}}}) & \check{\boldsymbol{B}} \cdot [(\boldsymbol{v}^{\mathrm{ref}} - \boldsymbol{n}^{\mathrm{q}} \cdot \boldsymbol{q}) \cdot \sin\boldsymbol{\delta}]^{n^{\mathrm{g}}} - \check{\boldsymbol{G}}[(\boldsymbol{v}^{\mathrm{ref}} - \boldsymbol{n}^{\mathrm{q}} \cdot \boldsymbol{q}) \cdot \cos\boldsymbol{\delta}]^{n^{\mathrm{g}}} \end{bmatrix} \tag{12}$$

$$\frac{\partial \mathbf{g}}{\partial \boldsymbol{z}} = \begin{bmatrix} I^{n^{\mathrm{g}}} + \check{\boldsymbol{G}} \cdot [\boldsymbol{r_c}]^{n^{\mathrm{g}}} - \check{\boldsymbol{B}} \cdot [\boldsymbol{x_c}]^{n^{\mathrm{g}}} & -\check{\boldsymbol{G}} \cdot [\boldsymbol{x_c}]^{n^{\mathrm{g}}} - \check{\boldsymbol{B}} \cdot [\boldsymbol{r_c}]^{n^{\mathrm{g}}} \\ \check{\boldsymbol{B}} \cdot [\boldsymbol{r_c}]^{n^{\mathrm{g}}} + \check{\boldsymbol{G}} \cdot [\boldsymbol{x_c}]^{n^{\mathrm{g}}} & I^{n^{\mathrm{g}}} + \check{\boldsymbol{G}} \cdot [\boldsymbol{r_c}]^{n^{\mathrm{g}}} - \check{\boldsymbol{B}} \cdot [\boldsymbol{x_c}]^{n^{\mathrm{g}}} \end{bmatrix} \tag{13}$$

Authorized licensed use limited to: Washington State University. Downloaded on October 11,2022 at 18:27:39 UTC from IEEE Xplore. Restrictions apply.

The OPF in (1), with additional constraints (16)–(23), constitute an SSSC-OPF for an inverter-dominant microgrid. The constraints (1b)–(1g) are quadratic functions of the bus voltage $\boldsymbol{v}$. The state matrix $\hat{\boldsymbol{A}}$ in (16) and the constraints (21) and (23) are nonlinear functions of $\boldsymbol{i}^{\mathrm{o}}$, $\boldsymbol{q}$, and $\boldsymbol{\delta}$. These nonlinearities make the problem nonconvex. In the next section, the SSSC-OPF problem is lifted and relaxed to make it computationally tractable.

III. Lifting, Relaxation, and Penalization

A. Lifted Formulation

The constraints (1b)–(1g) can be convexified by defining an auxiliary matrix $\boldsymbol{W} \in \mathbb{H}^n$ [31] as

$$\boldsymbol{W} \triangleq \boldsymbol{v}\boldsymbol{v}^*. \tag{24}$$

To convexify the constraints (21) and (23), and the state matrix $\hat{\boldsymbol{A}}$ in (16), variables $\boldsymbol{\delta}^{\mathrm{c}} \in \mathbb{R}^{n_{\mathrm{g}}\times 1}$, $\boldsymbol{\delta}^{\mathrm{s}} \in \mathbb{R}^{n_{\mathrm{g}}\times 1}$, $\boldsymbol{\delta}^{\mathrm{qc}} \in \mathbb{R}^{n_{\mathrm{g}}\times 1}$, $\boldsymbol{\delta}^{\mathrm{qs}} \in \mathbb{R}^{n_{\mathrm{g}}\times 1}$, and a new vector, $\boldsymbol{u}_k \in \mathbb{R}^{n_u\times 1}\ \forall\, k \in \mathcal{G}$, are defined for each inverter as

$$\boldsymbol{\delta}^{\mathrm{c}} \triangleq \cos\boldsymbol{\delta}, \qquad \boldsymbol{\delta}^{\mathrm{s}} \triangleq \sin\boldsymbol{\delta} \tag{25a}$$

$$\boldsymbol{\delta}^{\mathrm{qc}} \triangleq \boldsymbol{q}\cdot\cos\boldsymbol{\delta},\ \boldsymbol{\delta}^{\mathrm{qs}} \triangleq \boldsymbol{q}\cdot\sin\boldsymbol{\delta} \tag{25b}$$

$$\boldsymbol{u}_k \triangleq [i_k^{\mathrm{od}}, i_k^{\mathrm{oq}}, \delta_k^{\mathrm{c}}, \delta_k^{\mathrm{s}}, q_k, \delta_k^{\mathrm{qc}}, \delta_k^{\mathrm{qs}}]^\top\ \forall k \in \mathcal{G}. \tag{25c}$$

Using (25c), an auxiliary matrix for each inverter, $\boldsymbol{X}_k \in \mathbb{S}^{n_u}\ \forall\, k \in \mathcal{G}$, is defined as

$$\boldsymbol{X}_k \triangleq \boldsymbol{u}_k\boldsymbol{u}_k^\top \tag{25d}$$

that satisfies a set of constraints $\mathcal{U}$ given as

$$(\boldsymbol{e}_k^{\delta^{\mathrm{s}}})^\top \boldsymbol{X}_k \boldsymbol{e}_k^{q} - \delta_k^{\mathrm{qs}} = 0 \tag{26a}$$

$$(\boldsymbol{e}_k^{\delta^{\mathrm{c}}})^\top \boldsymbol{X}_k \boldsymbol{e}_k^{q} - \delta_k^{\mathrm{qc}} = 0 \tag{26b}$$

$$(\boldsymbol{e}_k^{\delta^{\mathrm{c}}})^\top \boldsymbol{X}_k \boldsymbol{e}_k^{\delta^{\mathrm{qs}}} - (\boldsymbol{e}_k^{\delta^{\mathrm{s}}})^\top \boldsymbol{X}_k \boldsymbol{e}_k^{\delta^{\mathrm{qc}}} = 0 \tag{26c}$$

$$(\boldsymbol{e}_k^{\delta^{\mathrm{c}}})^\top \boldsymbol{X}_k \boldsymbol{e}_k^{\delta^{\mathrm{c}}} + (\boldsymbol{e}_k^{\delta^{\mathrm{s}}})^\top \boldsymbol{X}_k \boldsymbol{e}_k^{\delta^{\mathrm{s}}} - 1 = 0 \tag{26d}$$

$$(\boldsymbol{e}_k^{\delta^{\mathrm{c}}})^\top \boldsymbol{X}_k \boldsymbol{e}_k^{\delta^{\mathrm{qc}}} + (\boldsymbol{e}_k^{\delta^{\mathrm{s}}})^\top \boldsymbol{X}_k \boldsymbol{e}^{\delta_k^{\mathrm{qs}}} - q_k = 0 \tag{26e}$$

$$(\boldsymbol{e}_k^{\delta^{\mathrm{qc}}})^\top \boldsymbol{X}_k \boldsymbol{e}_k^{\delta^{\mathrm{qc}}} + (\boldsymbol{e}_k^{\delta^{\mathrm{qs}}})^\top \boldsymbol{X}_k \boldsymbol{e}_k^{\delta^{\mathrm{qs}}} - (\boldsymbol{e}_k^{q})^\top \boldsymbol{X}_k \boldsymbol{e}_k^{q} = 0 \tag{26f}$$

where $\boldsymbol{e}_k^{i^{\mathrm{od}}}$, $\boldsymbol{e}_k^{i^{\mathrm{od}}}$, $\boldsymbol{e}_k^{\delta^{\mathrm{c}}}$, $\boldsymbol{e}_k^{\delta^{\mathrm{s}}}$, $\boldsymbol{e}_k^{q}$, $\boldsymbol{e}_k^{\delta^{\mathrm{qc}}}$, and $\boldsymbol{e}_k^{\delta^{\mathrm{qs}}}$ are the standard bases for respective elements of the vector $\boldsymbol{u}_k$.

From (24) and (25d), the constraints (1b)-(1g), (21), (23) and submatrices $\boldsymbol{A}(\boldsymbol{i}^{\mathrm{od}}, \boldsymbol{i}^{\mathrm{oq}}, \boldsymbol{\delta}, \boldsymbol{q})$, $\boldsymbol{B}(\boldsymbol{\delta}, \boldsymbol{q})$, and $\boldsymbol{C}(\boldsymbol{\delta}, \boldsymbol{q})$ can be reformulated as the linear functions of $\boldsymbol{u}_k$ and $\boldsymbol{X}_k$ as in (28)–(30). The state matrix $\hat{\boldsymbol{A}}$ and the stability constraint (16) are still nonlinear, due to the presence of $\boldsymbol{B}(\boldsymbol{D})^{-1}\boldsymbol{C}$, $\hat{\boldsymbol{A}}^\top\boldsymbol{M}$, and $\boldsymbol{M}\hat{\boldsymbol{A}}$ terms. To overcome this, two auxiliary matrices, $\boldsymbol{E}$ and $\boldsymbol{L}$, are defined

$$\boldsymbol{E} = \begin{bmatrix} \boldsymbol{E}^{\mathrm{bb}} & \boldsymbol{E}^{\mathrm{bc}} \\ \boldsymbol{E}^{\mathrm{cb}} & \boldsymbol{E}^{\mathrm{cc}} \end{bmatrix} \triangleq \begin{bmatrix} \boldsymbol{B}(\boldsymbol{\delta}^{\mathrm{c}}, \boldsymbol{\delta}^{\mathrm{s}}, \boldsymbol{\delta}^{\mathrm{qc}}, \boldsymbol{\delta}^{\mathrm{qs}}) \\ \hat{\boldsymbol{C}}^\top(\boldsymbol{\delta}^{\mathrm{c}}, \boldsymbol{\delta}^{\mathrm{s}}, \boldsymbol{\delta}^{\mathrm{qc}}, \boldsymbol{\delta}^{\mathrm{qs}}) \end{bmatrix} \begin{bmatrix} \boldsymbol{B}(\boldsymbol{\delta}^{\mathrm{c}}, \boldsymbol{\delta}^{\mathrm{s}}, \boldsymbol{\delta}^{\mathrm{qc}}, \boldsymbol{\delta}^{\mathrm{qs}}) \\ \hat{\boldsymbol{C}}^\top(\boldsymbol{\delta}^{\mathrm{c}}, \boldsymbol{\delta}^{\mathrm{s}}, \boldsymbol{\delta}^{\mathrm{qc}}, \boldsymbol{\delta}^{\mathrm{qs}}) \end{bmatrix}^\top \tag{27a}$$

$$\boldsymbol{L} = \begin{bmatrix} \boldsymbol{L}^{\mathrm{mm}} & \boldsymbol{L}^{\mathrm{ma}} \\ \boldsymbol{L}^{\mathrm{am}} & \boldsymbol{L}^{\mathrm{aa}} \end{bmatrix} \triangleq \begin{bmatrix} \boldsymbol{M} \\ \hat{\boldsymbol{A}}^\top \end{bmatrix} [\boldsymbol{M}, \hat{\boldsymbol{A}}] \tag{27b}$$

where $\hat{\boldsymbol{C}}(\boldsymbol{\delta}^{\mathrm{c}}, \boldsymbol{\delta}^{\mathrm{s}}, \boldsymbol{\delta}^{\mathrm{qc}}, \boldsymbol{\delta}^{\mathrm{qs}}) = (\boldsymbol{D})^{-1}\boldsymbol{C}(\boldsymbol{\delta}^{\mathrm{c}}, \boldsymbol{\delta}^{\mathrm{s}}, \boldsymbol{\delta}^{\mathrm{qc}}, \boldsymbol{\delta}^{\mathrm{qs}})$. $\boldsymbol{D}$ is a constant matrix for a given distribution network.

The lifted formulation of the SSSC-OPF is given in (28), where (28b)–(28l) are linear and convex. The nonconvexity present in the original SSSC-OPF is encapsulated by the constraints (28o)–(28r).

$$\text{minimize} \quad \mathrm{h}(\boldsymbol{p}^{\mathrm{g}}) \tag{28a}$$

subject to

OPF constraints:

$$\boldsymbol{G}^\top(\boldsymbol{p} + j\boldsymbol{q}) = \hat{\boldsymbol{D}}^\top\boldsymbol{d} + \mathrm{diag}\{\boldsymbol{W}\boldsymbol{Y}^*\} \tag{28b}$$

$$\mathrm{diag}\{\vec{\boldsymbol{L}}\,\boldsymbol{W}\vec{\boldsymbol{Y}}^*\} \le \boldsymbol{f}^{\max} \tag{28c}$$

$$\mathrm{diag}\{\overleftarrow{\boldsymbol{L}}\,\boldsymbol{W}\overleftarrow{\boldsymbol{Y}}^*\} \le \boldsymbol{f}^{\max} \tag{28d}$$

$$\boldsymbol{p}^{\min} \le \boldsymbol{p} \le \boldsymbol{p}^{\max} \tag{28e}$$

$$\boldsymbol{q}^{\min} \le \boldsymbol{q} \le \boldsymbol{q}^{\max} \tag{28f}$$

$$(\boldsymbol{v}^{\min})^2 \le \mathrm{diag}(\boldsymbol{W}) \le (\boldsymbol{v}^{\max})^2 \tag{28g}$$

$$\boldsymbol{i}^{\mathrm{o}} = \boldsymbol{G}^\top\boldsymbol{Y}\boldsymbol{v} \tag{28h}$$

$$\boldsymbol{G}^\top\boldsymbol{v} = \boldsymbol{v}^{\mathrm{ref}}\cdot(\boldsymbol{\delta}^{\mathrm{c}} + \mathrm{j}\boldsymbol{\delta}^{\mathrm{s}}) - \boldsymbol{n}^q\cdot(\boldsymbol{\delta}^{\mathrm{qc}} + \mathrm{j}\boldsymbol{\delta}^{\mathrm{qs}}) - \boldsymbol{i}^{\mathrm{o}}\cdot\boldsymbol{z}^c \tag{28i}$$

$$p_k + \mathrm{j}q_k = ((\boldsymbol{e}_k^{i^{\mathrm{od}}})^\top\boldsymbol{X}_k\boldsymbol{e}_k^{i^{\mathrm{od}}} + (\boldsymbol{e}_k^{i^{\mathrm{oq}}})^\top\boldsymbol{X}_k\boldsymbol{e}_k^{i^{\mathrm{oq}}})z_k^{\mathrm{c}} + p_k^g + \mathrm{j}q_k^g \quad \forall\, k \in \mathcal{G} \tag{28j}$$

Stability constraints:

$$\boldsymbol{L}^{\mathrm{am}} + \boldsymbol{L}^{\mathrm{ma}} \preceq -2\eta\boldsymbol{M} \tag{28k}$$

$$\boldsymbol{M} \succeq \mathbf{I}^{\boldsymbol{n_x}} \tag{28l}$$

Auxiliary variable constraints:

$$\hat{\boldsymbol{A}} = \boldsymbol{A}(\boldsymbol{X}_k) - \boldsymbol{E} \quad \forall\, k \in \mathcal{G} \tag{28m}$$

$$\boldsymbol{u}_k = [i_k^{\mathrm{od}}, i_k^{\mathrm{oq}}, \delta_k^{\mathrm{c}}, \delta_k^{\mathrm{s}}, q_k, \delta_k^{\mathrm{qc}}, \delta_k^{\mathrm{qs}}]^\top\ \forall k \in \mathcal{G} \tag{28n}$$

$$\boldsymbol{W} = \boldsymbol{v}\boldsymbol{v}^* \tag{28o}$$

$$\begin{bmatrix} \boldsymbol{E}^{\mathrm{bb}} & \boldsymbol{E}^{\mathrm{bc}} \\ \boldsymbol{E}^{\mathrm{cb}} & \boldsymbol{E}^{\mathrm{cc}} \end{bmatrix} = \begin{bmatrix} \boldsymbol{B}(\boldsymbol{\delta}^{\mathrm{c}}, \boldsymbol{\delta}^{\mathrm{s}}, \boldsymbol{\delta}^{\mathrm{qc}}, \boldsymbol{\delta}^{\mathrm{qs}}) \\ \hat{\boldsymbol{C}}^\top(\boldsymbol{\delta}^{\mathrm{c}}, \boldsymbol{\delta}^{\mathrm{s}}, \boldsymbol{\delta}^{\mathrm{qc}}, \boldsymbol{\delta}^{\mathrm{qs}}) \end{bmatrix} \begin{bmatrix} \boldsymbol{B}(\boldsymbol{\delta}^{\mathrm{c}}, \boldsymbol{\delta}^{\mathrm{s}}, \boldsymbol{\delta}^{\mathrm{qc}}, \boldsymbol{\delta}^{\mathrm{qs}}) \\ \hat{\boldsymbol{C}}^\top(\boldsymbol{\delta}^{\mathrm{c}}, \boldsymbol{\delta}^{\mathrm{s}}, \boldsymbol{\delta}^{\mathrm{qc}}, \boldsymbol{\delta}^{\mathrm{qs}}) \end{bmatrix}^\top \tag{28p}$$

$$\begin{bmatrix} \boldsymbol{L}^{\mathrm{mm}} & \boldsymbol{L}^{\mathrm{ma}} \\ \boldsymbol{L}^{\mathrm{am}} & \boldsymbol{L}^{\mathrm{aa}} \end{bmatrix} = \begin{bmatrix} \boldsymbol{M} \\ \hat{\boldsymbol{A}}^\top \end{bmatrix} [\boldsymbol{M}\ \hat{\boldsymbol{A}}] \tag{28q}$$

$$\boldsymbol{X}_k = [i_k^{\mathrm{od}}, i_k^{\mathrm{oq}}, \delta_k^{\mathrm{c}}, \delta_k^{\mathrm{s}}, q_k, \delta_k^{\mathrm{qc}}, \delta_k^{\mathrm{qs}}]^\top [i_k^{\mathrm{od}}, i_k^{\mathrm{oq}}, \delta_k^{\mathrm{c}}, \delta_k^{\mathrm{s}}, q_k, \delta_k^{\mathrm{qc}}, \delta_k^{\mathrm{qs}}] \quad \forall\, k \in \mathcal{G} \tag{28r}$$

$$\boldsymbol{X}_k, [i_k^{\mathrm{od}}, i_k^{\mathrm{oq}}, \delta_k^{\mathrm{c}}, \delta_k^{\mathrm{s}}, q_k, \delta_k^{\mathrm{qc}}, \delta_k^{\mathrm{qs}}]^\top \in \mathcal{U} \quad \forall\, k \in \mathcal{G}$$

variables

Authorized licensed use limited to: Washington State University. Downloaded on October 11,2022 at 18:27:39 UTC from IEEE Xplore. Restrictions apply.

$\boldsymbol{v} \in \mathbb{C}^{n\times 1}$, $\boldsymbol{p}^{\mathrm{g}} \in \mathbb{R}^{n^{\mathrm{g}}\times 1}$, $\boldsymbol{q}^{\mathrm{g}} \in \mathbb{R}^{n^{\mathrm{g}}\times 1}$, $\boldsymbol{i}^{\mathrm{o}} \in \mathbb{C}^{n^{\mathrm{g}}\times 1}$,

$\boldsymbol{q} \in \mathbb{R}^{n^{\mathrm{g}}\times 1}$, $\boldsymbol{\delta}^{\mathrm{c}} \in \mathbb{R}^{n^{\mathrm{g}}\times 1}$, $\boldsymbol{\delta}^{\mathrm{s}} \in \mathbb{R}^{n^{\mathrm{g}}\times 1}$, $\boldsymbol{\delta}^{\mathrm{qc}} \in \mathbb{R}^{n^{\mathrm{g}}\times 1}$,

$\boldsymbol{\delta}^{\mathrm{qs}} \in \mathbb{R}^{n^{\mathrm{g}}\times 1}$, $\boldsymbol{M} \in \mathbb{S}^{n^{\mathrm{g}}}$, $\boldsymbol{W} \in \mathbb{H}^{n}$, $\hat{\boldsymbol{A}} \in \mathbb{R}^{n_{\mathrm{x}}\times n_{\mathrm{x}}}$,

$$\boldsymbol{E}=\begin{bmatrix}\boldsymbol{E}^{\mathrm{bb}} & \boldsymbol{E}^{\mathrm{bc}}\\ \boldsymbol{E}^{\mathrm{cb}} & \boldsymbol{E}^{\mathrm{cc}}\end{bmatrix}\in \mathbb{R}^{2n_{\mathrm{x}}\times 2n_{\mathrm{x}}},\ \boldsymbol{L}=\begin{bmatrix}\boldsymbol{L}^{\mathrm{mm}} & \boldsymbol{L}^{\mathrm{ma}}\\ \boldsymbol{L}^{\mathrm{am}} & \boldsymbol{L}^{\mathrm{aa}}\end{bmatrix}\in \mathbb{R}^{2n_{\mathrm{x}}\times 2n_{\mathrm{x}}},$$

and $\boldsymbol{X}_k \in \mathbb{R}^{n_u\times n_u}\forall\, k \in \mathcal{G}$.

where

$\mathcal{U}$ is set of constraints defined as (26),

The matrices $\boldsymbol{A}(\boldsymbol{X}_k)$, $\boldsymbol{B}(\boldsymbol{\delta}^{\mathrm{c}}, \boldsymbol{\delta}^{\mathrm{s}}, \boldsymbol{\delta}^{\mathrm{qc}}, \boldsymbol{\delta}^{\mathrm{qs}})$, and $\boldsymbol{C}(\boldsymbol{\delta}^{\mathrm{c}}, \boldsymbol{\delta}^{\mathrm{s}}, \boldsymbol{\delta}^{\mathrm{qc}}, \boldsymbol{\delta}^{\mathrm{qs}})$ are defined as (29), (30), and (30), respectively. (28s)

B. Convex Relaxation

To ensure that (28) is computationally tractable, nonconvex constraints (28o)–(28r) are relaxed. This article details two distinct relaxation approaches, an SDP relaxation and a computationally efficient parabolic relaxation.

1) SDP Relaxation: The SDP relaxation of the nonconvex constraints in the lifted SSSC-OPF problem (28) is given as

$$\boldsymbol{W}-\boldsymbol{v}\boldsymbol{v}^{*}\succeq 0 \tag{32a}$$

$$\begin{bmatrix}\boldsymbol{E}^{\mathrm{bb}} & \boldsymbol{E}^{\mathrm{bc}}\\ \boldsymbol{E}^{\mathrm{cb}} & \boldsymbol{E}^{\mathrm{cc}}\end{bmatrix}-\begin{bmatrix}\boldsymbol{B}(\boldsymbol{\delta}^{\mathrm{c}}, \boldsymbol{\delta}^{\mathrm{s}}, \boldsymbol{\delta}^{\mathrm{qc}}, \boldsymbol{\delta}^{\mathrm{qs}})\\ \hat{\boldsymbol{C}}^{\top}(\boldsymbol{\delta}^{\mathrm{c}}, \boldsymbol{\delta}^{\mathrm{s}}, \boldsymbol{\delta}^{\mathrm{qc}}, \boldsymbol{\delta}^{\mathrm{qs}})\end{bmatrix}\begin{bmatrix}\boldsymbol{B}(\boldsymbol{\delta}^{\mathrm{c}}, \boldsymbol{\delta}^{\mathrm{s}}, \boldsymbol{\delta}^{\mathrm{qc}}, \boldsymbol{\delta}^{\mathrm{qs}})\\ \hat{\boldsymbol{C}}^{\top}(\boldsymbol{\delta}^{\mathrm{c}}, \boldsymbol{\delta}^{\mathrm{s}}, \boldsymbol{\delta}^{\mathrm{qc}}, \boldsymbol{\delta}^{\mathrm{qs}})\end{bmatrix}^{\top}\succeq 0 \tag{32b}$$

$$\begin{bmatrix}\boldsymbol{L}^{\mathrm{mm}} & \boldsymbol{L}^{\mathrm{ma}}\\ \boldsymbol{L}^{\mathrm{am}} & \boldsymbol{L}^{\mathrm{aa}}\end{bmatrix}-\begin{bmatrix}\boldsymbol{M}\\ \hat{\boldsymbol{A}}^{\top}\end{bmatrix}[\boldsymbol{M}, \hat{\boldsymbol{A}}]\succeq 0 \tag{32c}$$

$$\boldsymbol{X}_k-\boldsymbol{u}_k{\boldsymbol{u}_k}^{\top}\succeq 0\quad \forall\, k\in\mathcal{G}. \tag{32d}$$

Remark 1: The constraints (31a)–(31d) can be cast as

$$\begin{bmatrix}\boldsymbol{W} & \boldsymbol{v}\\ \boldsymbol{v}^{*} & 1\end{bmatrix}\succeq 0 \tag{33}$$

$$\begin{bmatrix}\boldsymbol{E}^{\mathrm{bb}} & \boldsymbol{E}^{\mathrm{bc}} & \boldsymbol{B}^{\top}(\boldsymbol{\delta}^{\mathrm{c}}, \boldsymbol{\delta}^{\mathrm{s}}, \boldsymbol{\delta}^{\mathrm{qc}}, \boldsymbol{\delta}^{\mathrm{qs}})\\ \boldsymbol{E}^{\mathrm{cb}} & \boldsymbol{E}^{\mathrm{cc}} & \hat{\boldsymbol{C}}^{\top}(\boldsymbol{\delta}^{\mathrm{c}}, \boldsymbol{\delta}^{\mathrm{s}}, \boldsymbol{\delta}^{\mathrm{qc}}, \boldsymbol{\delta}^{\mathrm{qs}})\\ \boldsymbol{B}^{\top}(\boldsymbol{\delta}^{\mathrm{c}}, \boldsymbol{\delta}^{\mathrm{s}}, \boldsymbol{\delta}^{\mathrm{qc}}, \boldsymbol{\delta}^{\mathrm{qs}}) & \hat{\boldsymbol{C}}(\boldsymbol{\delta}^{\mathrm{c}}, \boldsymbol{\delta}^{\mathrm{s}}, \boldsymbol{\delta}^{\mathrm{qc}}, \boldsymbol{\delta}^{\mathrm{qs}}) & \mathbf{I}^{n_z}\end{bmatrix}\succeq 0 \tag{34}$$

$$\begin{bmatrix}\boldsymbol{L}^{\mathrm{mm}} & \boldsymbol{L}^{\mathrm{ma}} & \boldsymbol{M}\\ \boldsymbol{L}^{\mathrm{am}} & \boldsymbol{L}^{\mathrm{aa}} & \hat{\boldsymbol{A}}^{\top}\\ \boldsymbol{M} & \hat{\boldsymbol{A}} & \mathbf{I}^{n_x}\end{bmatrix}\succeq 0 \tag{35}$$

$$\begin{bmatrix}\boldsymbol{X}_k & \boldsymbol{u}_k\\ \boldsymbol{u}_k^{\top} & 1\end{bmatrix}\succeq 0\quad \forall k\in\mathcal{G}. \tag{36}$$

The aforementioned remark transforms the quadratic matrix inequalities (31b)–(31d) to convex linear matrix inequalities making the SSSC-OPF more tractable. Nevertheless, with the increase in the number of inverters and system size, solving the SSSC-OPF in (28) may become computationally challenging.

2) Parabolic Relaxation: This is an alternative relaxation technique with a reduced computational burden. The nonconvex problem is transformed to a convex quadratically constraint quadratic programming problem. The parabolic relaxation [31] of the nonconvex voltage constraint, (28o), is given by

$$|v_j+\ v_k|^2 \le W_{jj}+W_{kk}+\ (W_{kj}+W_{jk})\,\forall (j,k)\in\mathcal{L} \tag{37a}$$

$$|v_j-\ v_k|^2 \le W_{jj}+W_{kk}-\ (W_{kj}+W_{jk})\,\forall (j,k)\in\mathcal{L} \tag{37b}$$

$$|v_j+\mathrm{j}v_k|^2 \le W_{jj}+W_{kk}-\mathrm{j}(W_{kj}-W_{jk})\,\forall (j,k)\in\mathcal{L} \tag{37c}$$

$$|v_j-\mathrm{j}v_k|^2 \le W_{jj}+W_{kk}+\mathrm{j}(W_{kj}-W_{jk})\,\forall (j,k)\in\mathcal{L} \tag{37d}$$

$$|v_j|^2 \le W_{jj}\qquad \forall j\in\mathcal{N}. \tag{37e}$$

$$\boldsymbol{A}=\begin{bmatrix}-[\boldsymbol{\omega}^{\mathrm{c}}] & -\left[\left(\omega_k^{\mathrm{c}} n_k^{\mathrm{q}}((\boldsymbol{e}_k^{i^{\mathrm{oq}}})^{\top}\boldsymbol{X}_k\boldsymbol{e}_k^{\delta^{\mathrm{s}}}+(\boldsymbol{e}_k^{i^{\mathrm{od}}})^{\top}\boldsymbol{X}_k\boldsymbol{e}_k^{\delta^{\mathrm{c}}})\right)_{k\in\mathcal{G}}\right] & -\left[\left(\omega_k^{\mathrm{c}}(v_k^{\mathrm{ref}}((\boldsymbol{e}_k^{i^{\mathrm{oq}}})^{\top}\boldsymbol{X}_k\boldsymbol{e}_k^{\delta^{\mathrm{s}}}+(\boldsymbol{e}_k^{i^{\mathrm{od}}})^{\top}\boldsymbol{X}_k\boldsymbol{e}_k^{\delta^{\mathrm{c}}}))\right)_{k\in\mathcal{G}}\right]+\\ & & \left[\left(\omega_k^{\mathrm{c}} n_k^{\mathrm{q}}(((\boldsymbol{e}_k^{i^{\mathrm{oq}}})^{\top}\boldsymbol{X}_k\boldsymbol{e}_k^{\delta^{\mathrm{qs}}}+(\boldsymbol{e}_k^{i^{\mathrm{od}}})^{\top}\boldsymbol{X}_k\boldsymbol{e}_k^{\delta^{\mathrm{qc}}}))\right)_{k\in\mathcal{G}}\right]\\ 0^{n^{\mathrm{g}}} & \left[\left(\omega_k^{\mathrm{c}} n_k^{\mathrm{q}}((\boldsymbol{e}_k^{i^{\mathrm{oq}}})^{\top}\boldsymbol{X}_k\boldsymbol{e}_k^{\delta^{\mathrm{c}}}-(\boldsymbol{e}_k^{i^{\mathrm{od}}})^{\top}\boldsymbol{X}_k\boldsymbol{e}_k^{\delta^{\mathrm{s}}})-\omega_k^{\mathrm{c}}\right)_{k\in\mathcal{G}}\right] & \left[\left(\omega_k^{\mathrm{c}}(v_k^{\mathrm{ref}}((\boldsymbol{e}_k^{i^{\mathrm{od}}})^{\top}\boldsymbol{X}_k\boldsymbol{e}_k^{\delta^{\mathrm{c}}}+(\boldsymbol{e}_k^{i^{\mathrm{oq}}})^{\top}\boldsymbol{X}_k\boldsymbol{e}_k^{\delta^{\mathrm{s}}}))\right)_{k\in\mathcal{G}}\right]-\\ & & \left[\left(\omega_k^{\mathrm{c}} n_k^{\mathrm{q}}(((\boldsymbol{e}_k^{i^{\mathrm{od}}})^{\top}\boldsymbol{X}_k\boldsymbol{e}_k^{\delta^{\mathrm{qc}}}+(\boldsymbol{e}_k^{i^{\mathrm{oq}}})^{\top}\boldsymbol{X}_k\boldsymbol{e}_k^{\delta^{\mathrm{qs}}}))\right)_{k\in\mathcal{G}}\right]\\ \boldsymbol{M}^{\mathrm{p}} & 0^{n^{\mathrm{g}}-1} & 0^{n^{\mathrm{g}}-1}\end{bmatrix} \tag{29}$$

$$\boldsymbol{B}=\begin{bmatrix}\begin{bmatrix}\left(\omega_k^{\mathrm{c}}(v_k^{\mathrm{ref}}\delta_k^{\mathrm{c}}-n_k^{\mathrm{q}}\delta_k^{\mathrm{qc}})\right)_{k\in\mathcal{G}}\\ \left(\omega_k^{\mathrm{c}}(v_k^{\mathrm{ref}}\delta_k^{\mathrm{s}}-n_k^{\mathrm{q}}\delta_k^{\mathrm{qs}})\right)_{k\in\mathcal{G}}\end{bmatrix} & \begin{bmatrix}\left(\omega_k^{\mathrm{c}}(v_k^{\mathrm{ref}}\delta_k^{\mathrm{s}}-n_k^{\mathrm{q}}\delta_k^{\mathrm{qs}})\right)_{k\in\mathcal{G}}\\ -\left[\left(\omega_k^{\mathrm{c}}(v_k^{\mathrm{ref}}\delta_k^{\mathrm{c}})-n_k^{\mathrm{q}}\delta_k^{\mathrm{qc}})\right)_{k\in\mathcal{G}}\right]\end{bmatrix}\\ 0^{n\mathrm{g}-1} & 0^{n\mathrm{g}-1}\end{bmatrix} \tag{30}$$

$$\hat{\boldsymbol{C}}=\boldsymbol{D}^{-1}\begin{bmatrix}0^{n_{\mathrm{g}}} & \check{\boldsymbol{G}}\cdot[(n_k^{\mathrm{q}}\delta_k^{\mathrm{c}})_{k\in\mathcal{G}}]^{n^{\mathrm{g}}}-\check{\boldsymbol{B}}\cdot[(n_k^{\mathrm{q}}\delta_k^{\mathrm{s}})_{k\in\mathcal{G}}]^{n^{\mathrm{g}}} & \check{\boldsymbol{G}}\cdot[(v_k^{\mathrm{ref}}\delta_k^{\mathrm{s}}-n_k^{\mathrm{q}}\delta_k^{\mathrm{qs}})_{k\in\mathcal{G}}]^{n^{\mathrm{g}}}+\check{\boldsymbol{B}}\cdot[(v^{\mathrm{ref}_k}\delta_k^{\mathrm{c}}-n_k^{\mathrm{q}}\delta_k^{\mathrm{qc}})_{k\in\mathcal{G}}]^{n^{\mathrm{g}}}\\ 0^{n_{\mathrm{g}}} & \check{\boldsymbol{G}}\cdot[(n_k^{\mathrm{q}}\delta_k^{\mathrm{s}})_{k\in\mathcal{G}}]^{n^{\mathrm{g}}}+\check{\boldsymbol{B}}\cdot[(n_k^{\mathrm{q}}\delta_k^{\mathrm{c}})_{k\in\mathcal{G}}]^{n^{\mathrm{g}}} & \check{\boldsymbol{B}}\cdot[(v_k^{\mathrm{ref}}\delta_k^{\mathrm{s}}-n_k^{\mathrm{q}}\delta_k^{\mathrm{qs}})_{k\in\mathcal{G}}]^{n^{\mathrm{g}}}-\check{\boldsymbol{G}}[(v^{\mathrm{ref}_k}\delta_k^{\mathrm{c}}-n_k^{\mathrm{q}}\delta_k^{\mathrm{qc}})_{k\in\mathcal{G}}]^{n^{\mathrm{g}}}\end{bmatrix} \tag{31}$$

Authorized licensed use limited to: Washington State University. Downloaded on October 11,2022 at 18:27:39 UTC from IEEE Xplore. Restrictions apply.

The parabolic relaxation of (28p)–(28r) can be obtained using the following proposition.

Proposition 2: Assume $\boldsymbol{R} \in \mathbb{R}^{r\times s}$, $\boldsymbol{S} \in \mathbb{R}^{s\times r}$, and $\boldsymbol{T} \in \mathbb{S}^{2r}$ are the matrices expressed by

$$\boldsymbol{T} = \begin{bmatrix} \boldsymbol{T}^{\mathrm{rr}} & \boldsymbol{T}^{\mathrm{rs}} \\ \boldsymbol{T}^{\mathrm{sr}} & \boldsymbol{T}^{\mathrm{ss}} \end{bmatrix} = [\boldsymbol{R}^{\top},\, \boldsymbol{S}]^{\top}[\boldsymbol{R}^{\top},\, \boldsymbol{S}]. \tag{37f}$$

The parabolic relaxation [24] is formulated as

$$T^{\mathrm{rr}}_{jj} + T^{\mathrm{ss}}_{kk} + 2\,T^{\mathrm{rs}}_{jk} \geq \|\boldsymbol{r}_j + \boldsymbol{s}_k\|^2 \;\forall j,k \in \{1,2,..,r\} \tag{37g}$$

$$T^{\mathrm{rr}}_{jj} + T^{\mathrm{ss}}_{kk} - 2\,T^{\mathrm{rs}}_{jk} \geq \|\boldsymbol{r}_j - \boldsymbol{s}_k\|^2 \;\forall j,k \in \{1,2,..,r\}. \tag{37h}$$

Here, $\boldsymbol{r}_j$ and $\boldsymbol{s}_k$ are the jth and kth column vectors of the matrices $\boldsymbol{R}$ and $\boldsymbol{S}^{\top}$, respectively.

Proposition 2 convexifies the nonlinear matrix equality constraints given by (28p)–(28r) using the parabolic relaxation technique. This approach relaxes the nonconvex SSSC-OPF problem into a tractable SSSC-OPF problem. While the relaxed SSSC-OPF problem is computationally tractable, it may not guarantee a feasible solution for the original problem in (1). Therefore, a sequential penalization approach is adopted.

C. Sequential Penalization

The solution obtained from the lifted problem (28a)–(28m) with the relaxed SSSC-OPF constraints (32)–(35) or (36a)–(36h) may not be always feasible with the original problem (1). To resolve this, a linear penalty function ρ is added to the objective function in (28a)

$$\text{minimize}\, \mathrm{h}(\boldsymbol{p}^{\mathrm{g}}) + \rho(\boldsymbol{W}, \boldsymbol{v}, \boldsymbol{E}, \boldsymbol{B}, \hat{\boldsymbol{C}}, \boldsymbol{L}, \boldsymbol{M}, \hat{\boldsymbol{A}}, \boldsymbol{X}, \boldsymbol{u}) \tag{38a}$$

$$\text{subject to (28b)–(28m)} \tag{38b}$$

$$\text{(33)–(36) SDP-relaxed constraints} \tag{38c}$$

$$\text{or}$$

$$\text{(37a)–(37h) Parabolic-relaxed constraints} \tag{38d}$$

where

$$\rho(\boldsymbol{W}, \boldsymbol{v}, \boldsymbol{E}, \boldsymbol{B}, \hat{\boldsymbol{C}}, \boldsymbol{L}, \boldsymbol{M}, \hat{\boldsymbol{A}}, \boldsymbol{X}, \boldsymbol{u}) \tag{39}$$

$$\begin{aligned} \triangleq\; & (\mathrm{tr}\{\boldsymbol{W}\boldsymbol{P}\} - \boldsymbol{v}_0^{*}\boldsymbol{P}\boldsymbol{v} - \boldsymbol{v}^{*}\boldsymbol{P}\boldsymbol{v}_0 + \boldsymbol{v}_0^{*}\boldsymbol{P}\boldsymbol{v}_0) + \mu_1(\mathrm{tr}\{\boldsymbol{E}\} - \\ & 2\mathrm{tr}\{\boldsymbol{B}_0\boldsymbol{B}^{\top}\} - 2\mathrm{tr}\{\hat{\boldsymbol{C}}_0\hat{\boldsymbol{C}}^{\top}\} + \mathrm{tr}\{\boldsymbol{B}_0\boldsymbol{B}_0^{\top}\} + \mathrm{tr}\{\hat{\boldsymbol{C}}_0\hat{\boldsymbol{C}}_0^{\top}\}) \\ & \mu_2(\mathrm{tr}\{\boldsymbol{L}\} - 2\mathrm{tr}\{\boldsymbol{M}_0\boldsymbol{M}^{\top}\} - 2\mathrm{tr}\{\hat{\boldsymbol{A}}_0\hat{\boldsymbol{A}}^{\top}\} + \mathrm{tr}\{\boldsymbol{M}_0\boldsymbol{M}_0^{\top}\} \\ & + \mathrm{tr}\{\hat{\boldsymbol{A}}_0\hat{\boldsymbol{A}}_0^{\top}\}) + \mu_3\mathrm{tr}\{\boldsymbol{X}_k - 2\boldsymbol{u}_{0_k}\boldsymbol{u}_k^{\top} + \boldsymbol{u}_{0_k}\boldsymbol{u}_{0_k}^{\top}\} \end{aligned} \tag{40}$$

where $\boldsymbol{v}_0, \boldsymbol{B}_0, \hat{\boldsymbol{C}}_0, \boldsymbol{M}_0, \hat{\boldsymbol{A}}_0,$ and $\boldsymbol{u}_{0_k}$ are the given initial values. μ_1, μ_2, and μ_3 are the penalty positive coefficients valued at 0.1, 0.5, and 5, respectively. Here, $\boldsymbol{P}$ is the penalty function coefficient matrix for the voltage, which can be calculated as in [31].

For an arbitrary initial point, the SSSC-OPF (38) is solved sequentially until a feasible solution to (1) is obtained. It can then reduce the value of the objective function in subsequent iterations until a near optimal solution is found [24], [25]. The penalized SSSC-OPF is solved till the ε is less than the considered threshold value. Here, ε is given as

$$\begin{aligned} \varepsilon = \max(&||\boldsymbol{v} - \boldsymbol{v}_0||, ||\boldsymbol{B} - \boldsymbol{B}_0||, ||\hat{\boldsymbol{C}} - \hat{\boldsymbol{C}}_0|| \\ &||\boldsymbol{M} - \boldsymbol{M}_0||, ||\hat{\boldsymbol{A}} - \hat{\boldsymbol{A}}_0||, ||\boldsymbol{u}_k - \boldsymbol{u}_{0_k}||). \end{aligned} \tag{41}$$

IV. Validation and Verification

A. Numerical Studies

The efficacy of both SDP and parabolic convex relaxations are evaluated on several standard test systems and also compared with the PENLAB [32] optimization tool. All numerical studies are performed in the MATLAB/CVX platform using MOSEK solver [33], on a 64-bit personal computer (PC) with 3.4-GHz Intel i7 quadcore processor and 64-GB RAM. The droop constants $\boldsymbol{m}^{\mathrm{p}} = 1.5 \times 10^{-4}$ and $\boldsymbol{n}^{\mathrm{q}} = 7.2 \times 10^{-4}$, and the minimum decay rate of $\eta = 1$, are chosen.

In Table I, upper bound (UB) indicates the optimal cost obtained after sequential penalization, lower bound (LB) indicates the optimal cost obtained for the relaxed problem without penalty, and computational time indicates the time taken by the optimization solver to reach the upper bound. In PENLAB, solving time indicates the time taken by the solver to obtain the optimal solution. From Table I, the solver time is significantly larger with PENLAB solver compared to the SDP and Parabolic relaxation methods. Further, for smaller systems with less number of inverters, the SDP relaxation offers LBs closer to the optimal solution with a similar computational time as compared to parabolic relaxation. As the number of inverters and system size increases, SDP becomes computationally more expensive.

B. Hardware-in-The-Loop Validation

The proposed SSSC-OPF is tested on a four-bus, four-inverter microgrid system [34], shown in Fig. 4. The microgrid's base power and voltage are 0.1 MVA and 480 V, respectively. The nominal frequency of the microgrid is $\omega_{\mathrm{nom}} = 377$ rd/s and the generator cost coefficients with their power limits are tabulated in Table II. This microgrid has variable-impedance loads, with 0.707 lagging power factor, at all buses. The complete microgrid is emulated in two Typhoon HIL604 units. Inverters employ droop control schemes with $\boldsymbol{m}^{\mathrm{p}} = 1.04 \times 10^{-4}$ (for the active power-frequency droop) and $\boldsymbol{n}^{\mathrm{q}} = 2.3 \times 10^{-4}$ (for the reactive power-voltage droop). These controllers are realized using two dSPACE MLBx control boxes with a 100-μs sampling rate. A personal computer (PC) with an 8-core, 3.5 GHz Xeon processor, and 64-GB RAM solves the SSSC-OPF using MATLAB/CVX optimization tool with an MOSEK solver [33]. The stability constraint threshold in the SSSC-OPF is chosen as $\eta = 1$. The PC reads the microgrid information from the HIL emulator every two minutes, solves the penalized relaxed SSSC-OPF problem, and sends the optimal solution to the control boxes. The information sharing between the HIL emulator and the PC, and the PC and control boxes, is carried out using Ethernet communication.

1) Microgrid Performance With the Conventional Droop Control and With the SSSC-OPF: The microgrid system is

Authorized licensed use limited to: Washington State University. Downloaded on October 11,2022 at 18:27:39 UTC from IEEE Xplore. Restrictions apply.

TABLE I
UPPER BOUNDS, LOWER BOUNDS, AND COMPUTATIONAL TIMES FOR SSSC-OPF WITH SDP AND PARABOLIC RELAXATIONS AND THEIR COMPARISON WITH PENLAB [32] OPTIMIZATION TOOL SOLUTION

Test system	n^g	UB	SDP		Parabolic		PENLAB	
			LB	time (s)	LB	time (s)	Optimal solution	Solving time (s)
9-bus	3	4234.76	3984.51	0.44	3900.42	0.42	4234.77	1294
14-bus	5	7963.32	7076.86	0.61	6561.84	0.53	7963.34	2287
30-bus	6	563.15	523.77	0.95	498.90	0.61	-	-
57-bus	7	43728.37	39803.98	2.88	35740.58	1.26	-	-
39-bus	10	39241.56	33307.43	6.83	32607.87	3.33	-	-
89pegase	12	5830.64	5127.92	19.95	4226.49	8.69	-	-
24_ieee_rts	33	-	56877.63	3487.61	53263.30	728.30	-	-

TABLE II
GENERATIONAL COST COEFFICIENTS AND POWER LIMITS

Bus	c_2	c_1	c_0	$p^{\min}$	$p^{\max}$	$q^{\min}$	$q^{\max}$
1	1.3	2.2	0	0	1.0	-0.80	0.80
2	1.6	2.8	0	0	1.0	-0.80	0.80
3	2.0	5.5	0	0	1.0	-0.80	0.80
4	1.6	2.4	0	0	1.0	-0.80	0.80

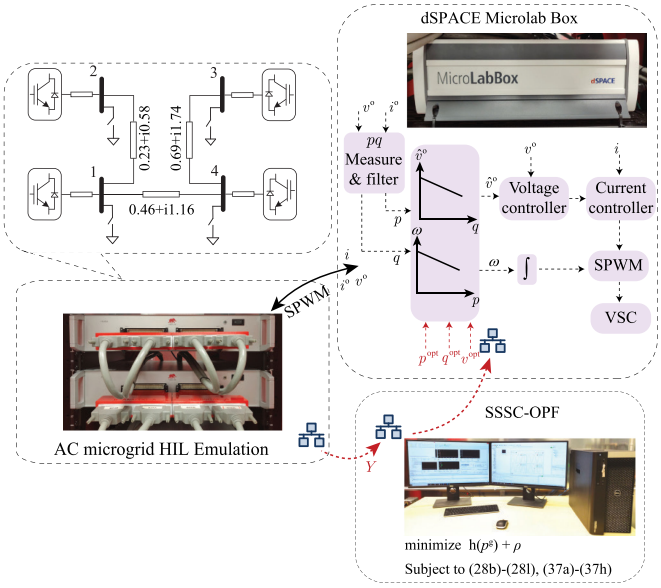

Fig. 4. Microgrid test system implemented using HIL (Typhoon HIL), control unit (dSPACE), and optimization unit (personal computer), with information flow shown.

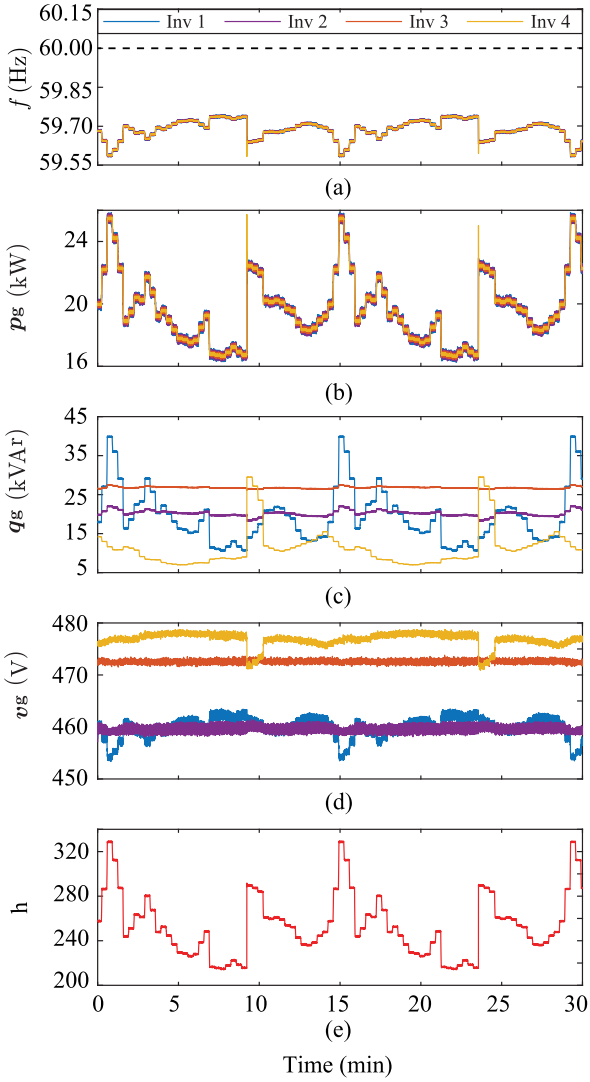

Fig. 5. Operation with droop control and varying loads at bus 1 and 4. (a) Frequency. (b) Active power generation. (c) Reactive power generation. (d) Voltage magnitude. (e) Total generation cost.

emulated in the HIL environment for 30 min. Every 20 s, loads at all buses are randomly varied following a Poisson distribution. Figs. 5 and 6 depict the microgrid operation without and with the SSSC-OPF, respectively. Without the SSSC-OPF, the set-point values were held constant at $\boldsymbol{p}^{\text{opt}} = 0$, $\boldsymbol{q}^{\text{opt}} = 0$, and $\boldsymbol{v}^{\text{opt}} = 480\,V$. The voltages and the reactive power generations are within the limits for both scenarios, as shown in Fig. 5(c) and (d) and Fig. 6(c) and (d). The active power load variations are shared equally among all the inverters due to the constant active power set-point ($\boldsymbol{p}^{\text{opt}}$) and identical droop constants ($\boldsymbol{m}^{\text{p}}$), as shown in Fig. 5(b). On the contrary, using the SSSC-OPF, the optimal set points are provided at every 2 min, leading to unequal, but cost effective powers supplied by the inverters, as shown in Fig. 6(b). The average total generation cost for 30 min, with the droop control alone, is 253.5723. Using the SSSC-OPF, the average total generation cost reduces to 233.7836. Fig. 7 shows the traces of eigenvalues at different optimal set points provided by the SSSC-OPF under varying load conditions. It can be observed that the real part of eigenvalues are always kept less than -1, which is expected as $\eta = 1$. As per the IEEE 1547 [35] the microgrid control strategy, the frequency deviation of the microgrid needs to be acceptable to all associated parties. The capability of the microgrid system to maintain a tight frequency

Authorized licensed use limited to: Washington State University. Downloaded on October 11,2022 at 18:27:39 UTC from IEEE Xplore. Restrictions apply.

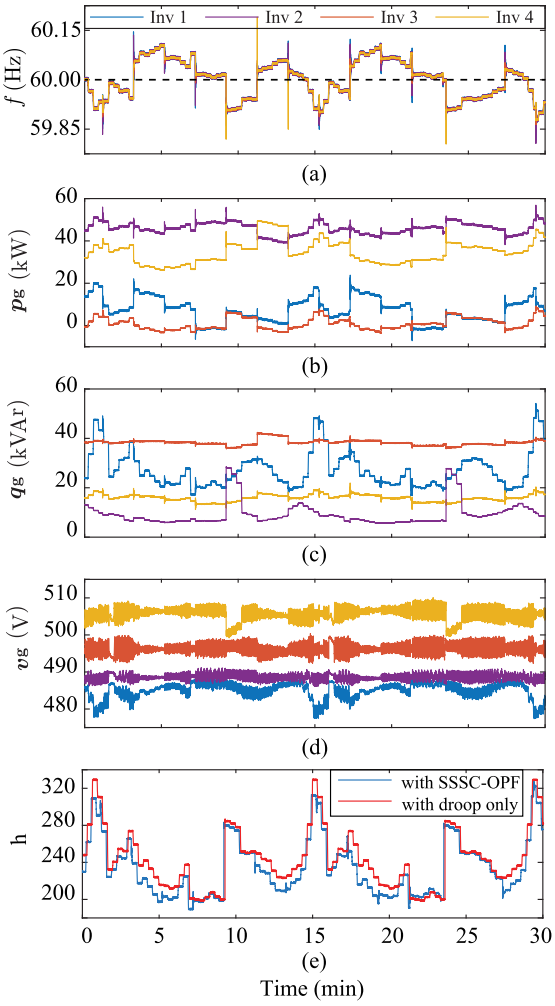

Fig. 6. Microgrid operation with the SSSC-OPF and varying loads at bus 1 and 4. (a) Frequency. (b) Active power generation. (c) Reactive power generation. (d) Voltage magnitude. (e) Total generation cost.

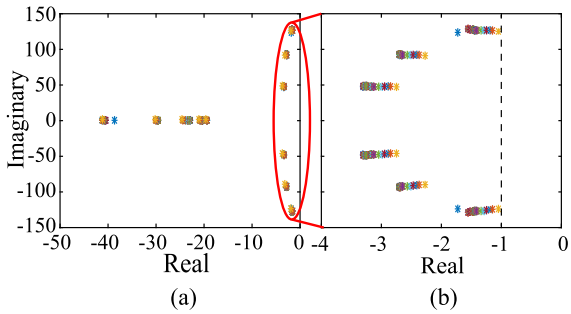

Fig. 7. (a) Microgrid eigenvalues with varying load conditions under the SSSC-OPF. (b) Zoomed-in view of the plot.

range will dictate the ability for load following. From Figs. 5(a) and 6(a), it can be observed that the operating frequency, with the droop control alone, deviates further from the nominal value ($f_{\text{nom}} = 60$ Hz) compared to when the SSSC-OPF is employed.

2) Comparing the Conventional OPF and SSSC-OPF: The advantage of the SSSC-OPF over the conventional OPF is demonstrated here. Figs. 8 and 9 portray the microgrid

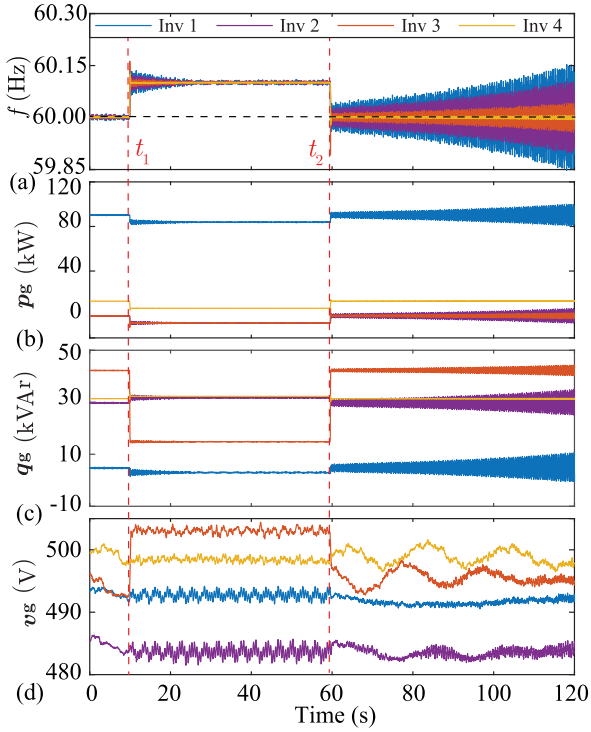

Fig. 8. Microgrid performance with optimal set points provided by the conventional OPF with the load at bus 3 disconnected and reconnected at $t = t_1$ and $t = t_2$. (a) Frequency. (b) Active power generation. (c) Reactive power generation. (d) Voltage magnitude.

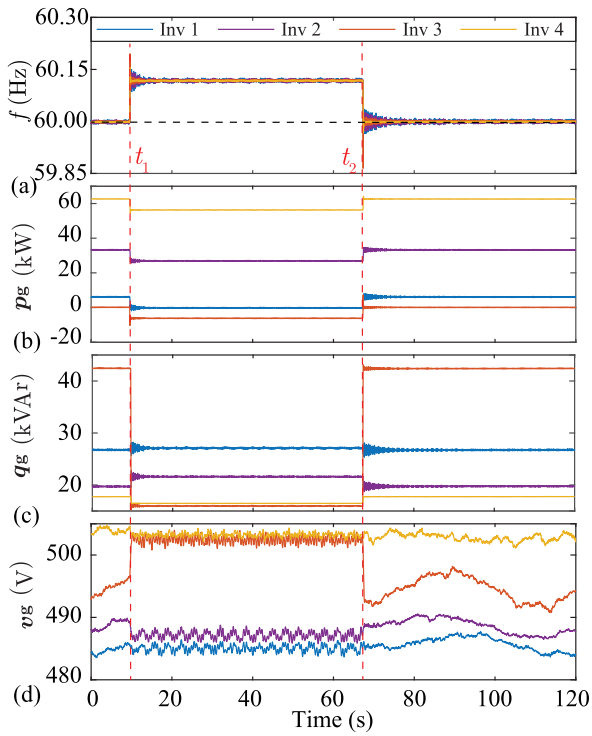

Fig. 9. Microgrid performance with optimal set points provided by the SSSC-OPF with the load at bus 3 disconnected and reconnected at $t = t_1$ and $t = t_2$. (a) Frequency. (b) Active power generation. (c) Reactive power generation. (d) Voltage magnitude.

Authorized licensed use limited to: Washington State University. Downloaded on October 11,2022 at 18:27:39 UTC from IEEE Xplore. Restrictions apply.

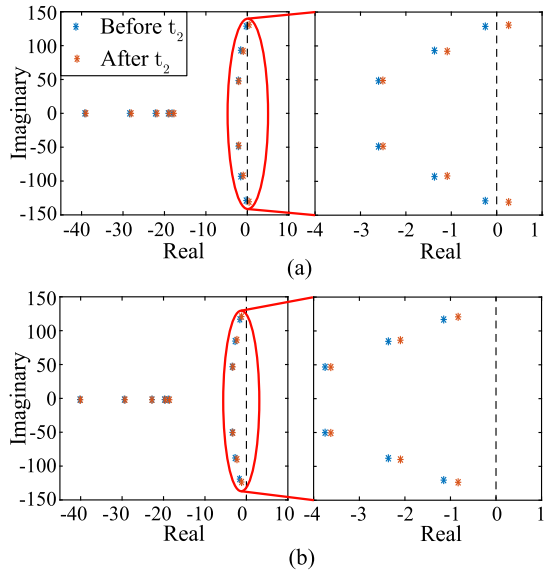

Fig. 10. Microgrid eigenvalues under (a) OPF and (b) SSSC-OPF. * indicates eigenvalues before the load disturbance at $t = t_2$ and * indicates eigenvalues after $t = t_2$.

performance with the operating set points dictated by the OPF and SSSC-OPF, respectively. In both scenarios, initially, the microgrid operates with load impedance of $(5 + i5)\,\Omega$ at all buses. At $t = t_1$, the load at bus 3 is disconnected. Set points provided by the SSSC-OPF lead to better damping as compared to that of the conventional OPF, as observed from Figs. 8(a) and 9(a). At $t = t_2$, the load is added back to bus 3. The microgrid driven by the OPF exhibits negative damping leading to an oscillatory instability, while the SSSC-OPF provides stable operation with a positive damping. Microgrid eigenvalues, under the OPF and SSSC-OPF, are shown in Fig. 10(a) and (b), respectively. Under the conventional OPF, two eigenvalues are very close to the imaginary axis, which with a small perturbation in load, could shift to the right side of the imaginary axis and make the microgrid unstable. By contrast, under the SSSC-OPF, the eigenvalues are further away from the imaginary axis to provide a stability margin.

V. Conclusion

This article addressed the stable and optimal operation of inverter-populated ac microgrids. The SSSC-OPF provided the optimal operating set points to the inverters and exhibited improved damping characteristics as compared to the operation provided by the conventional OPF. The stability constraints for the SSSC-OPF was formulated as a BMI constraint derived from a Lyapunov stability candidate. The SSSC-OPF formulation was nonconvex due to the presence of multiple nonlinear terms. To make it computationally efficient, we have relaxed this problem using two distinct convex relaxation techniques, namely, SDP and parabolic relaxations. To prove solution scalability, several numerical studies were carried out on multiple standard IEEE and European test systems. Further, the feasibility and the efficacy of the proposed SSSC-OPF was evaluated on a microgrid system emulated in a CHIL setup.

References

[1] G. Agundis-Tinajero *et al.*, "Extended-optimal-power-flow-based hierarchical control for islanded AC microgrids," *IEEE Trans. Power Electron.*, vol. 34, no. 1, pp. 840–848, Jan. 2019.

[2] N. Pogaku, M. Prodanovic, and T. C. Green, "Modeling, analysis and testing of autonomous operation of an inverter-based microgrid," *IEEE Trans. Power Electron.*, vol. 22, no. 2, pp. 613–625, Mar. 2007.

[3] R. Majumder, "Some aspects of stability in microgrids," *IEEE Trans. Power Syst.*, vol. 28, no. 3, pp. 3243–3252, Aug. 2013.

[4] R. Majumder, B. Chaudhuri, A. Ghosh, R. Majumder, G. Ledwich, and F. Zare, "Improvement of stability and load sharing in an autonomous microgrid using supplementary droop control loop," *IEEE Trans. Power Syst.*, vol. 25, no. 2, pp. 796–808, May 2010.

[5] A. Kahrobaeian and Y. A. I. Mohamed, "Analysis and mitigation of low-frequency instabilities in autonomous medium-voltage converter-based microgrids with dynamic loads," *IEEE Trans. Ind. Electron.*, vol. 61, no. 4, pp. 1643–1658, Apr. 2014.

[6] A. Firdaus and S. Mishra, "Mitigation of power and frequency instability to improve load sharing among distributed inverters in microgrid systems," *IEEE Syst. J.*, vol. 14, no. 1, pp. 1024–1033, Mar. 2020.

[7] A. Trivedi and M. Singh, "l_1 adaptive droop control for AC microgrid with small mesh network," *IEEE Trans. Ind. Electron.*, vol. 65, no. 6, pp. 4781–4789, Jun. 2018.

[8] X. Guo, Z. Lu, B. Wang, X. Sun, L. Wang, and J. M. Guerrero, "Dynamic phasors-based modeling and stability analysis of droop-controlled inverters for microgrid applications," *IEEE Trans. Smart Grid*, vol. 5, no. 6, pp. 2980–2987, Nov. 2014.

[9] D. K. Dheer, V. A. S, O. V. Kulkarni, and S. Doolla, "Improvement of stability margin of droop-based islanded microgrids by cascading of lead compensators," *IEEE Trans. Ind. Appl.*, vol. 55, no. 3, pp. 3241–3251, May 2019.

[10] A. Pizano-Martianez, C. R. Fuerte-Esquivel, and D. Ruiz-Vega, "Global transient stability-constrained optimal power flow using an OMIB reference trajectory," *IEEE Trans. Power Syst.*, vol. 25, no. 1, pp. 392–403, Feb. 2010.

[11] B. Cui and X. A. Sun, "A new voltage stability-constrained optimal power-flow model: Sufficient condition, SOCP representation, and relaxation," *IEEE Trans. Power Syst.*, vol. 33, no. 5, pp. 5092–5102, Sep. 2018.

[12] C. Wang, B. Cui, Z. Wang, and C. Gu, "SDP-based optimal power flow with steady-state voltage stability constraints," *IEEE Trans. Smart Grid*, vol. 10, no. 4, pp. 4637–4647, Jul. 2019.

[13] M. Nojavan and H. Seyedi, "Voltage stability constrained OPF in multi-micro-grid considering demand response programs," *IEEE Syst. J.*, vol. 14, no. 4, pp. 5221–5228, Dec. 2020.

[14] S. Nikkhah, M.-A. Nasr, and A. Rabiee, "A stochastic voltage stability constrained EMS for isolated microgrids in the presence of PEVs using a coordinated UC-OPF framework," *IEEE Trans. Ind. Electron.*, vol. 68, no. 5, pp. 4046–4055, May 2021.

[15] J. Condren and T. W. Gedra, "Expected-security-cost optimal power flow with small-signal stability constraints," *IEEE Trans. Power Syst.*, vol. 21, no. 4, pp. 1736–1743, Nov. 2006.

[16] R. Zarate-Minano, F. Milano, and A. J. Conejo, "An OPF methodology to ensure small-signal stability," *IEEE Trans. Power Syst.*, vol. 26, no. 3, pp. 1050–1061, Aug. 2011.

[17] P. Li, H. Wei, B. Li, and Y. Yang, "Eigenvalue-optimisation-based optimal power flow with small-signal stability constraints," *IET Gener., Transmiss. Distrib.*, vol. 7, no. 5, pp. 440–450, May 2013.

[18] P. Li, J. Qi, J. Wang, H. Wei, X. Bai, and F. Qiu, "An SQP method combined with gradient sampling for small-signal stability constrained OPF," *IEEE Trans. Power Syst.*, vol. 32, no. 3, pp. 2372–2381, May 2017.

[19] Y. Li, G. Geng, Q. Jiang, W. Li, and X. Shi, "A sequential approach for small signal stability enhancement with optimizing generation cost," *IEEE Trans. Power Syst.*, vol. 34, no. 6, pp. 4828–4836, Nov. 2019.

[20] P. Pareek and H. D. Nguyen, "Small-signal stability constrained optimal power flow: A convexification approach," 2019. [Online]. Available: https://arxiv.org/abs/1911.12001

[21] L. Luo and S. V. Dhople, "Spatiotemporal model reduction of inverter-based islanded microgrids," *IEEE Trans. Energy Convers.*, vol. 29, no. 4, pp. 823–832, Dec. 2014.

Authorized licensed use limited to: Washington State University. Downloaded on October 11,2022 at 18:27:39 UTC from IEEE Xplore. Restrictions apply.

[22] D. Henrion, J. Lofberg, M. Kocvara and M. Stingl, "Solving polynomial static output feedback problems with PENBMI," in *Proc. 44th IEEE Conf. Decision and Control*, pp. 7581–7586, Dec, 2005.
[23] K. Michal and S. Michael, "PENNON: Software for linear and nonlinear matrix inequalities," in *Handbook on Semidefinite, Conic and Polynomial Optimization*. Boston, MA, USA: Springer, 2012, pp. 755–791.
[24] M. Kheirandishfard, F. Zohrizadeh, and R. Madani, "Convex relaxation of bilinear matrix inequalities part I: Theoretical results," in *Proc. IEEE Conf. Decis. Control*, Dec. 2018, pp. 67–74.
[25] M. Kheirandishfard, F. Zohrizadeh, M. Adil, and R. Madani, "Convex relaxation of bilinear matrix inequalities part II: Applications to optimal control synthesis," in *Proc. IEEE Conf. Decis. Control*, Dec. 2018, pp. 75–82.
[26] X. Wu, C. Shen, and R. Iravani, "A distributed, cooperative frequency and voltage control for microgrids," *IEEE Trans. Smart Grid*, vol. 9, no. 4, pp. 2764–2776, Jul. 2018.
[27] G. Chen and E. Feng, "Distributed secondary control and optimal power sharing in microgrids," *IEEE/CAA J. Automatica Sinica*, vol. 2, no. 3, pp. 304–312, Jul. 2015.
[28] M. C. Chandorkar, D. M. Divan, and R. Adapa, "Control of parallel connected inverters in standalone AC supply systems," *IEEE Trans. Ind. Appl.*, vol. 29, no. 1, pp. 136–143, Jan./Feb. 1993.
[29] S. Boyd, L. E. Ghaoui, E. Feron, and V. Balakrishnan, *Linear Matrix Inequalities in System and Control Theory*. Philadelphia, PA, USA: SIAM, 1994.
[30] F. Mei and B. Pal, "Modal analysis of grid-connected doubly fed induction generators," *IEEE Trans. Energy Convers.*, vol. 22, no. 3, pp. 728–736, Sep. 2007.
[31] F. Zohrizadeh, M. Kheirandishfard, E. Q. Jnr, and R. Madani, "Penalized parabolic relaxation for optimal power flow problem," in *Proc. IEEE Conf. Decis. Control*, Dec. 2018, pp. 1616–1623.
[32] J. Fiala, M. Kočvara, and M. Stingl, "Penlab: A MATLAB solver for nonlinear semidefinite optimization," 2013, *arXiv:1311.5240*.
[33] ApS, Mosek. "Mosek optimization toolbox for matlab," Users Guide and Reference Manual, Version 4 (2019).
[34] A. Bidram, A. Davoudi, F. L. Lewis, and J. M. Guerrero, "Distributed cooperative secondary control of microgrids using feedback linearization," *IEEE Trans. Power Syst.*, vol. 28, no. 3, pp. 3462–3470, Aug. 2013.
[35] IEEE Guide for Design, Operation, and Integration of Distributed Resource Island Systems With Electric Power Systems, *IEEE Std. 1547.4-2011*, 2011.

Deepak Pullaguram (Member, IEEE) received the M.Tech. degree in power systems engineering from the National Institute of Technology Warangal, Hanamkonda, India, in 2014, and the Ph.D. degree in electrical engineering from the Indian Institute of Technology Delhi, New Delhi, India, in 2018.

From 2018 to 2019, he was a Faculty Research Fellow with the Department of Electrical Engineering, University of Texas Arlington, Arlington, TX, USA. He is currently an Assistant Professor with the Department of Electrical Engineering, National Institute of Technology Warangal. His research interests include renewable power generation, dynamics and control of ac/dc microgrids, and cybersecurity in microgrids

Ramtin Madani (Member, IEEE) received the Ph.D. degree in electrical engineering from Columbia University, New York, NY, USA, in 2015.

He was a Postdoctoral Scholar with the Department of Industrial Engineering and Operations Research, University of California, Berkeley, Berkeley, CA, USA, in 2016. He is an Assistant Professor with the Department of Electrical Engineering, University of Texas at Arlington, Arlington, TX, USA. His research interests include developing algorithms for optimization and control with applications in energy.

Tuncay Altun (Member, IEEE) received the B.Sc. and M.Sc. degrees in electrical engineering from the Yıldız Technical University, Istanbul, Turkey, in 2011 and 2014, respectively, and the Ph.D. degree in electrical engineering from the University of Texas at Arlington, Arlington, TX, USA, in 2020.

He was a Postdoctoral Research Associate with the Department of Electrical Engineering, University of Texas at Arlington. He is a Lecturer with the Department of Electrical and Electronics Engineering, University of Bozok, Yozgat, Turkey. His research interests include optimization and control for power systems applications, renewable or sustainable energy systems, microgrids, and HVdc transmission.

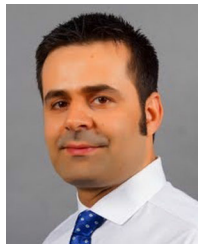

Ali Davoudi (Senior Member, IEEE) received the Ph.D. degree in electrical and computer engineering from the University of Illinois at Urbana-Champaign, Champaign, IL, USA, in 2010.

He is currently a Professor with the Electrical Engineering Department, University of Texas at Arlington, Arlington, TX, USA.

Dr. Davoudi is an Associate Editor for the IEEE TRANSACTIONS ON POWER ELECTRONICS and the Editor for the IEEE TRANSACTIONS ON ENERGY CONVERSION and IEEE POWER ENGINEERING LETTERS. He was the recipient of the the Best Paper Award from 2015 IEEE International Symposium on Resilient Control Systems, 2014–2015 Best Paper Award from the IEEE TRANSACTIONS ON ENERGY CONVERSION, 2016 Prize Paper Award from the IEEE Power and Energy Society, 2017 IEEE Richard M. Bass Outstanding Young Power Electronics Engineer Award, 2017–2018 Best Paper Award from the IEEE TRANSACTIONS ON ENERGY CONVERSION, 2019–2020 Faculty Fellow of Janet and Mike Greene Endowed Professorship, and 2019–2020 Best Paper Award from the IEEE TRANSACTIONS ON ENERGY CONVERSION (Electric Storage area).

Authorized licensed use limited to: Washington State University. Downloaded on October 11,2022 at 18:27:39 UTC from IEEE Xplore. Restrictions apply.